Journal of Medicinal Chemistry

pubs.acs.org/jmc

Drug Annotation

Discovery of Balovaptan, a Vasopressin 1a Receptor Antagonist for the Treatment of Autism Spectrum Disorder

Patrick Schnider,* Caterina Bissantz, Andreas Bruns, Cosimo Dolente, Erwin Goetschi, Roland Jakob-Roetne, Basil Künnecke, Thomas Mueggler, Wolfgang Muster, Neil Parrott, Emmanuel Pinard, Hasane Ratni, Céline Risterucci, Mark Rogers-Evans, Markus von Kienlin, and Christophe Grundschober

Cite This: https://dx.doi.org/10.1021/acs.jmedchem.9b01478

Read Online

ACCESS | Metrics & More | Article Recommendations | Supporting Information

ABSTRACT: We recently reported the discovery of a potent, selective, and brain-penetrant V1a receptor antagonist, which was not suitable for full development. Nevertheless, this compound was found to improve surrogates of social behavior in adults with autism spectrum disorder in an exploratory proof-of-mechanism study. Here we describe scaffold hopping that gave rise to triazolobenzodiazepines with improved pharmacokinetic properties. The key to balancing potency and selectivity while minimizing P-gp mediated efflux was fine-tuning of hydrogen bond acceptor basicity. Ascertaining a V1a antagonist specific brain activity pattern by pharmacological magnetic resonance imaging in the rat played a seminal role in guiding optimization efforts, culminating in the discovery of balovaptan (RG7314, RO5285119) **1**. In a 12-week clinical phase 2 study in adults with autism spectrum disorder balovaptan demonstrated improvements in Vineland-II Adaptive Behavior Scales, a secondary end point comprising communication, socialization, and daily living skills. Balovaptan entered phase 3 clinical development in August 2018.

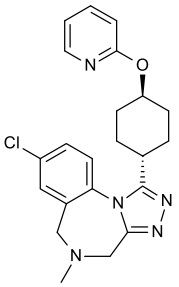

balovaptan (RG7314, RO5285119), 1

INTRODUCTION

Arginine vasopressin (AVP) is a 9 amino acid peptide activating G protein coupled receptors. Its functions include the regulation of water retention through the kidney vasopressin V2 receptor[1] and blood pressure through vascular smooth muscle V1a receptors.[2] In the brain it is mainly synthesized in the hypothalamic supraoptic and paraventricular nuclei and acts as a neurotransmitter regulating the HPA axis,[3] through the V1b receptor, and social and aggressive behavior through activation of the V1a receptor in brain areas implicated in social behavior.[4] The V1a receptor brain expression pattern has been shown to critically affect social behavior in voles.[5]

In humans promoter polymorphisms in the V1a gene have been associated with autism spectrum disorder,[6−11] and the V1a receptor is linked to social behavior. However, the exact role of vasopressin in autism has not been fully elucidated yet. Parker et al. showed that V1a receptor activation by intranasal administration of vasopressin improved social behavior in a small clinical study with 30 autistic children.[12] In contrast, intranasal administration of vasopressin impaired emotion recognition[13] and increased threat perception in healthy volunteers.[14] Recently we reported the discovery of the highly potent and selective brain-penetrant hV1a antagonist RO5028442 (RG7713), **2**.[15] A proof-of-mechanism study of this compound, given as a single infusion over 2 h to 19 adult men with autism spectrum disorder, demonstrated improvements in some exploratory biomarkers for social and communication behaviors, including a statistically significant increase in orienting preference to biological motion as assessed by eye tracking, a significantly reduced ability to detect lust, and a trend for reduced ability to detect fear.[16]

At the time, indole-3-carboxamides with spiro[1*H*-isobenzofuran-3,4′-piperidine] including **2** (Figure 1) stood out particularly for their unprecedented selectivity against oxytocin (OT) and vasopressin 2 (V2) receptors. While V2 selectivity is important to avoid side effects on water retention by the kidney,[1] avoidance of OT receptor antagonism is important since activation of the receptor is believed to have prosocial effects.[17] However, while **2** has a very good pharmacokinetic profile after intravenous administration to humans with a half-life of around 8 h,[16] the *in vivo* total blood clearance in animals is high, close to liver blood flow in the dog and exceeding liver blood flow in rat and mouse. It is thus not feasible to achieve sufficient exposures to establish robust safety margins in nonclinical studies, rendering this compound unsuitable for full

Received: September 5, 2019

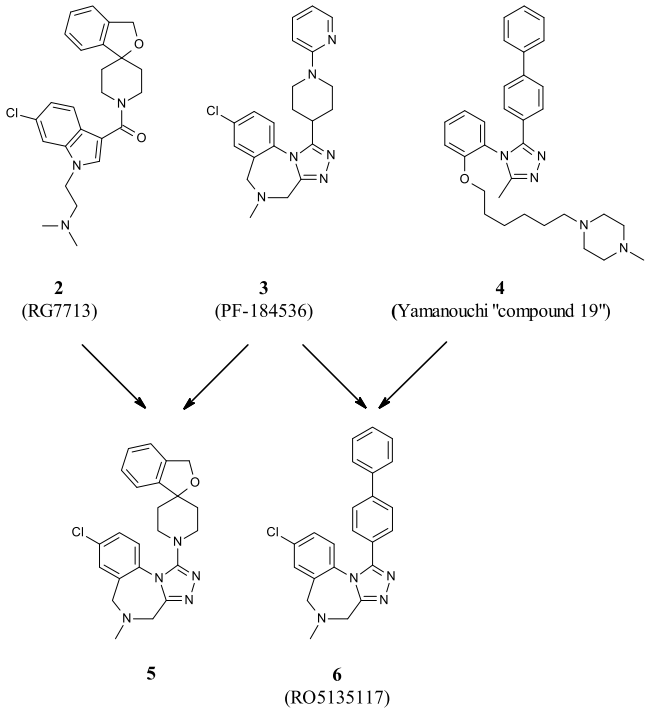

Figure 1. Known indole-3-carboxamide and 4-aryl-1,2,4-triazole V1a antagonists and hybrid design structures **5** and **6** (RO5135117).

development as an oral treatment. All attempts to improve metabolic stability in animals by modifications of the sterically exposed indole-*N*-substituent led to compounds with poor brain exposure due to P-glycoprotein (P-gp) mediated efflux. Since the identification of compounds from the indole-3-carboxamide class of V1a receptor antagonists that were simultaneously highly potent, selective, metabolically stable, and devoid of P-gp-mediated efflux turned out to be elusive,[15] we were prompted to explore a scaffold hop. To this end a 4-aryl substituted 1,2,4-triazole looked most promising since both **2** and the triazolobenzodiazepine PF-184563[18] **3** (Figure 1) feature a chlorophenyl group and a good H-bond acceptor (an amide carbonyl oxygen in the case of **2** and a 1,2,4-triazole nitrogen atom in **3**) at approximately the same distance, which suggested that these two classes of compounds might bind to V1a receptors in a similar way.

4-Aryl substituted 1,2,4-triazole derivatives were for the first time reported by researchers from Yamanouchi as potent and selective V1a receptor antagonists.[19] In a radioligand binding assay "compound 19" **4** (Figure 1) was reported to have 1700-fold selectivity for the human V1a vs the V2 receptor. In our hands, the selectivity of this compound in functional calcium-flux assays was found to be only 67-fold vs human V2 and 34-fold vs OT receptors (Table 2). In contrast, the triazolobenzodiazepine **3**[18] is more than 2400-fold selective against both human V2 and OT receptors (Table 1). However, the latter compound was also reported to have significant agonistic activity at V2 receptors,[18] which can lead to undesired antidiuretic side effects.[20] Moreover, **3** is a substrate of human P-gp with an efflux ratio of 4 and hence limited brain exposure. Nevertheless, the favorable *in vitro* as well as *in vivo* pharmacokinetic profile of **3** in rat[18] implied that the tricyclic

Table 1. *In Vitro* Potency, Selectivity, and Metabolic Stability Data of 3, 5, and Analogs of 5

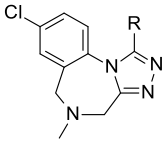

R =	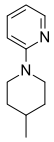	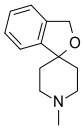	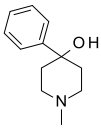	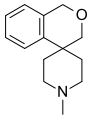	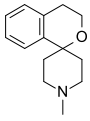	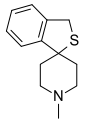	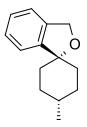	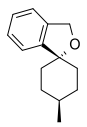
Cpd	**3**	**5**	**7**	**8**	**9**	**10**	**11**	**12**
hV1a pK_b[a]	8.9	9.6	8.6	9.3	8.8	9.0	9.1	9.2
fold selectivity vs hV2	2478	218	38	167	44	65	19	669
fold selectivity vs hOT	2415	127	35	14	10	9	5	236
HLM CL[b] (μL/min/mg Protein)	<10	<10	<10	22	<10	24	10	72
RLM CL[c] (μL/min/mg Protein)	72	718	435	949	550	493	206	1000

[a]pK_b: negative logarithm of the equilibrium dissociation constant measured in a calcium flux functional assay. [b]HLM CL: intrinsic clearance measured in human liver microsomes. [c]RLM CL: intrinsic clearance measured in rat liver microsomes.

https://dx.doi.org/10.1021/acs.jmedchem.9b01478
J. Med. Chem. XXXX, XXX, XXX−XXX

Table 2. *In Vitro* Potency and Selectivity Data of Compounds 4, 6, and Derivatives of 6

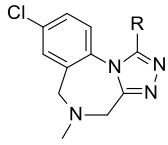

R =		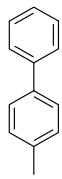	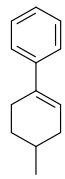	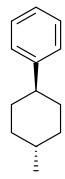	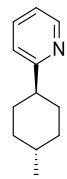
Cpd	**4**	**6**	**13**	**14**	**15**
hV1a pK_b[a]	8.7	8.6	9.3	9.5	9.6
LE[b]	0.32	0.42	0.46	0.47	0.47
fold selectivity vs hV2	67	30	90	17	1081
fold selectivity vs hOT	34	13	22	4	863

[a]pK_b: negative logarithm of the equilibrium dissociation constant measured in a calcium flux functional assay. [b]LE: ligand efficiency.

triazolobenzodiazepine was an attractive scaffold, while the conformationally much less restricted **4** has very low metabolic stability in human as well as rat liver microsomes. On the other hand, with a pK_b of 8.0, **4** features much higher potency at the rat V1a receptor compared to **3**, which has a pK_b of only 6.2. We thus hypothesized that replacement of the *N*-(pyridin-2-yl)piperidine "head-group" of this triazolobenzodiazepine derivative by different groups such as a biphenyl or a spiro[1*H*-isobenzofuran-3,4′-piperidine] group might give rise to potent and selective V1a receptor antagonists retaining an overall balanced pharmacokinetic profile suitable for an orally bioavailable brain penetrating drug (Figure 1, hybrid structures **5** and **6** (RO5135117)).

Herein we describe our efforts toward this end which culminated in the discovery of the 5,6-dihydro-4*H*-[1,2,4]-triazolo[4,3-*a*][1,4]benzodiazepinebalovaptan **1**. *In vivo* profiling using pharmacological magnetic resonance imaging (phMRI) in rats to record cerebral blood perfusion as a proxy for spatiotemporal patterns of evoked neural activity following drug administration[21] played a seminal role in guiding lead optimization efforts and the selection of **1** for clinical development. In a double-blind, randomized, placebo-controlled clinical phase 2 study in 223 adult men with autism spectrum disorder (VANILLA; NCT01793441) **1** was well tolerated and demonstrated dose-dependent and clinically meaningful improvements in the Vineland-II Adaptive Behavior Scales at oral doses of 4 mg and 10 mg daily, driven primarily by changes in the socialization and communication scores.[22] A phase 2 trial in children and adolescents (NCT02901431)[23] and a phase 3 trial in adult men and women (NCT03504917)[24] are both ongoing at the time of writing.

RESULTS AND DISCUSSION

Discovery of Balovaptan (1). The hybrid structure **5** was indeed found to be a potent V1a receptor antagonist (Table 1). However, the selectivity against V2 and OT receptors was an order of magnitude lower than that of **3**. Furthermore, **5** showed much higher clearance in rat liver microsomes than **3**, while metabolic turnover was low in human liver microsomes for both compounds.

Variation of the spiropiperidine group of **5** led to compounds **7**, **8**, **9**, and **10**, which had reduced potency and even lower selectivity. We therefore hypothesized that selectivity might be achievable in this class of V1a antagonists with head-groups attached to the triazole scaffold via an sp^3 carbon as in the highly selective PF-184563 **3**. Replacement of the spiro[1*H*-isobenzofuran-3,4′-piperidine] nitrogen of **5** by CH thus gave rise to the diastereomers **11** and **12** (Table 1). Although the latter was found not only to have the highest clearance of all compounds shown in Table 1 in rat liver microsomes but also high clearance in human liver microsomes, it indeed showed clearly increased selectivity as compared to **5**.

The second hybrid designed between the triazolobenzodiazepine PF-184563 **3** and the diphenyl substituted triazole **4**, compound **6** (RO5135117), retained potency as well. However, the selectivity against V2 and OT receptors was even lower than that of **4** (Table 2). Yet the finding that **6** is not a substrate of P-gp warranted further profiling of this compound. Indeed it was found that it had an acceptable pharmacokinetic profile in rats, with a clearance of 50−60% of liver blood flow and a V_{ss} of 4−6 L/kg, which resulted in a half-life of approximately 1.5 h after iv administration. Absorption was complete following oral administration, confirming the drug-like potential of this class of compounds. On the basis of extrapolation of unbound plasma concentrations and a K_b of 12 ± 6 nM at the rat V1a receptor, it was predicted that more than 90% brain V1a receptor occupancy should be achieved after iv injection of a single dose of 30 mg/kg in rats, and since a selectivity screen in a 50-target panel showed no off-target activities (see Supporting Information, Table 2), we selected this compound as a tool to probe the effect of central V1a receptor antagonism on brain circuitry in a preclinical phMRI study. In line with the prediction of the efficacious dose **6** indeed showed a strong modulation of brain circuitry in a

https://dx.doi.org/10.1021/acs.jmedchem.9b01478
J. Med. Chem. XXXX, XXX, XXX−XXX

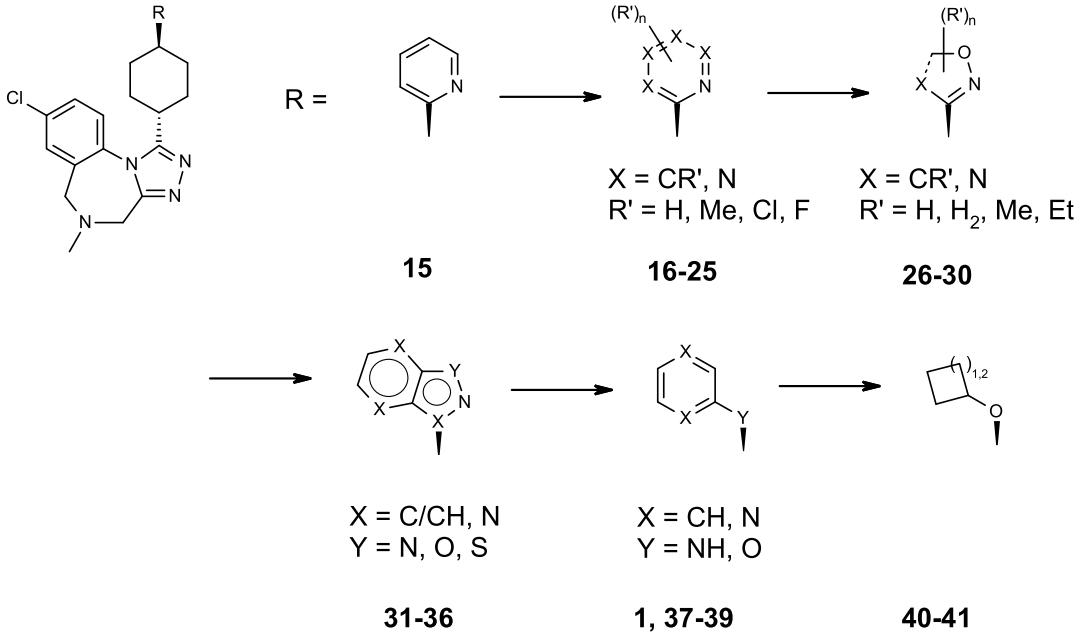

Figure 2. Evolution of the exploration of the effect of the polarity of R on P-gp mediated efflux. For detailed structures see Figure 3.

dose-dependent manner when tested in rat using arterial spin-labeling (ASL)[25] based phMRI as discussed in more detail below.

Encouraged by the *in vivo* profile of **6** and the preliminary evidence suggesting that selectivity may be achievable with head-groups attached to the triazole core via an sp^3 carbon, we envisaged saturation of the first phenyl ring of **6**. This gave rise to two compounds, the racemate **13** and **14**, with significantly increased potency at the human V1a receptor and excellent ligand efficiency but, disappointingly, no improved selectivity versus V2 and OT receptors (Table 2). Replacement of the phenyl ring of **14** by 2-pyridyl, however, led to a dramatic surge in selectivity, while V1a potency increased only slightly. Yet, like its close analog PF-184563 **3**, **15** is a substrate of human P-gp with a comparable efflux ratio of 4.4, while **14** is devoid of efflux. This result suggested that an H-bond acceptor in this part of the ligand is crucial for selectivity. At the same time the increase in polarity renders **15** a substrate of P-gp. Indeed the degree of hydrogen bond basicity was previously described as an important determinant of P-gp mediated efflux.[26−28]

The evolution of our efforts to explore replacements of the 2-pyridyl group of **15** (Table 2) in search of a compound that is devoid of P-gp mediated efflux is outlined in Figure 2. A set of 27 analogs differing only in the substituent in the 4-position of the cyclohexane ring were synthesized and tested in transfected LLC-PK1 cells expressing human P-gp. Linear regression analysis of a plot of the logarithm of the efflux ratio against log *D*, measured at pH 7.4, gave model 1 (Figure 3). In spite of a modest r^2 of 0.272, the efflux ratios of 22 of the 27 compounds were predicted with an error of less than 2-fold using this simplistic model.

$$\log 10\,(\text{efflux ratio}) = 1.07 - (0.25 \log D) \quad (1)$$

Lipophilicity is a composite of a volume and a polarity term. The latter is determined by dipolarizability, H-bond donor acidity, and H-bond acceptor basicity.[29] Volume and descriptors of polarity were also reported to be the main parameters predicting P-gp substrate specificity.[27] While it is thus plausible that log *D* is a useful predictor of the likelihood of P-gp mediated efflux, the data set described herein illustrates that more subtle effects such as steric accessability and efficiency of polar interactions with P-gp within the membrane may play an important role as discussed below.

Well in accordance with model 1, substitution of the pyridine ring of our lead structure **15** by fluoride, chloride, or methyl gave rise to compounds **16**−**21** with increased log *D* values between 2.5 and 3.2, all of which showed decreased efflux, while the pyridazine and pyrimidine analogs **22** and **23**, which are substantially more polar by 1.5 and 1.3 log units, respectively, showed stronger efflux. Unexpectedly, however, the dimethyl substituted pyrimidine **24**, which is 1 order of magnitude more lipophilic (log *D* = 2.0) than the unsubstituted pyrimidine derivative **23**, was found to be a very good substrate of P-gp. Interestingly, pyrazine (compound **25**) conferred substantial polarity without effecting efflux. This may be explicable by a reduced interaction with P-gp due to the modest hydrogen bond basicity of pyrazine (pK_{HB} = 1.22) as compared to, for example, pyridine (pK_{HB} = 1.86).[30]

A 5-methyl-1,2,4-oxadiazole ring (compound **26**) was found to be equipolar to pyrazine, giving even weaker P-gp mediated efflux. Again this is understandable by the low predicted H-bond basicity of the two nitrogen atoms (pK_{HB} = 0.5 and 0.4).[31] Replacing the oxadiazole N4 by CH raised log *D* by 0.6 units; yet the slightly increased efflux of the resulting isoxazole **27** as compared to oxadiazole **26** may be rationalized by the moderately higher H-bond basicity (pK_{HB} = 0.8[31]) of the isoxazole nitrogen. Addition of a second methyl group in position 4 of the isoxazole led to an increase in log *D* by 0.4 units as expected (compound **28**); similarly as for the pyrimidine−4,6-dimethylpyrimidine pair, methylation again led to a significant increase in the P-gp mediated efflux ratio from 2.4 to 3.8. It is not clear whether this is due to an increase in H-bond basicity by the introduction of the modestly electron-donating methyl group or rather a conformational effect. Conversely, the isomeric 5-ethylisoxazole **29**, which has almost the same log *D* but should have about the same H-bond basicity as the 5-methylisoxazole **27**, showed similarly low

https://dx.doi.org/10.1021/acs.jmedchem.9b01478
J. Med. Chem. XXXX, XXX, XXX−XXX

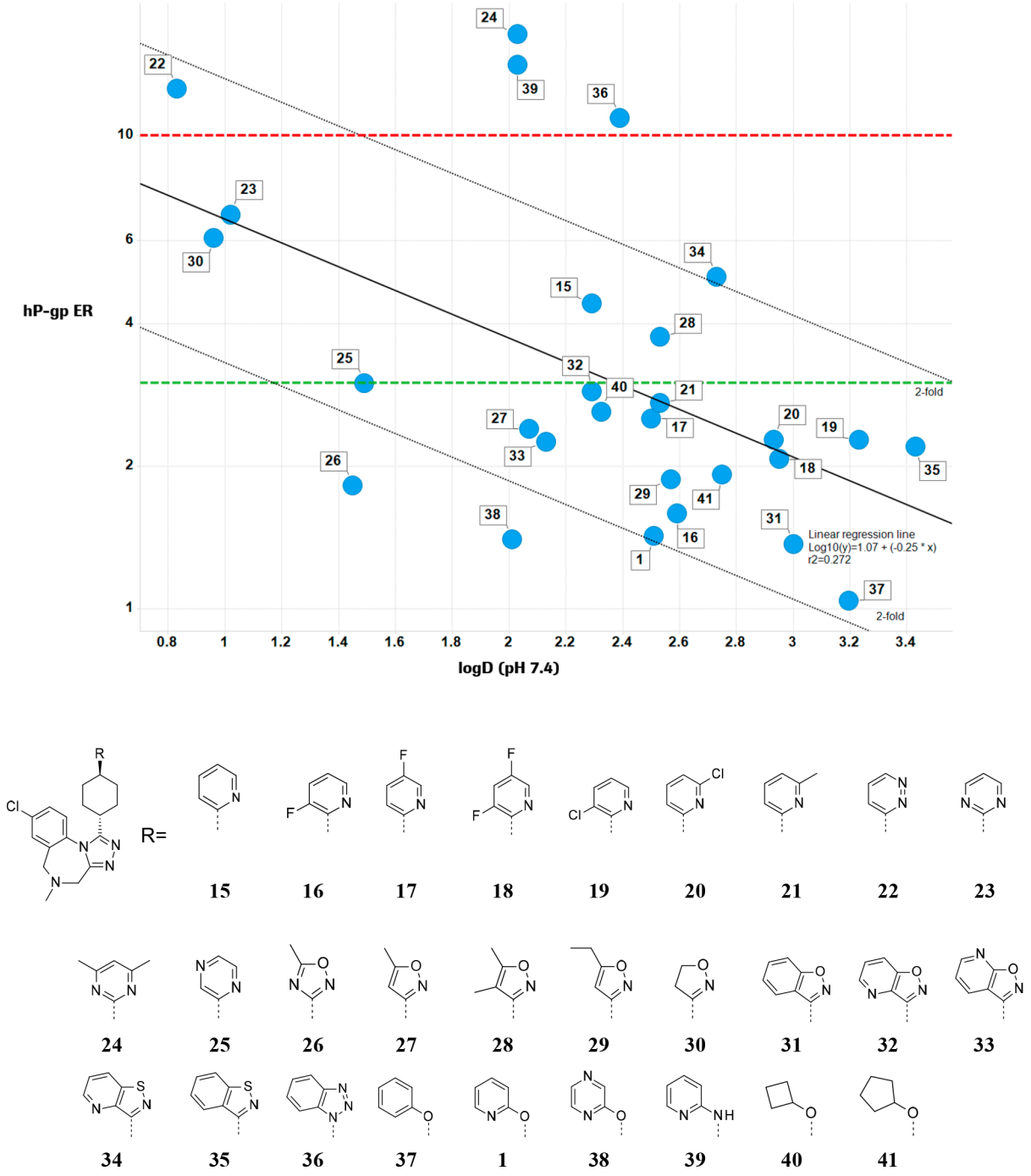

Figure 3. log *D* (pH 7.4) vs P-gp mediated efflux ratio (ER). Solid line: linear regression line. Dotted lines: within 2-fold of linear regression line. Green dotted line: ER = 3. Red dotted line: ER = 10.

efflux as the latter. Increasing electron density of the nitrogen and hence H-bond basicity by dearomatization gave the substantially polar 4,5-dihydroisoxazole **30**, which had a log *D* of 1 and hence an efflux ratio of 6.1.

Reducing the electron density of the isoxazole by fusion with a phenyl ring gave the benzisoxazole **31**, with a log *D* above 3 and no efflux (efflux ratio = 1.4). The two regioisomeric isoxazolopyridine analogs **32** and **33** were more polar by up to approximately 1 order of magnitude and showed slightly increased yet still modest efflux in accordance with model 1. It is worth noting that **34**, the isothiazole analog of **32**, was found to be a distinctly better substrate of P-gp in spite of its higher lipophilicity, presumably due to the lower electronegativity of sulfur as compared to oxygen, resulting in increased H-bond basicity of the adjacent nitrogen. The same trend was seen with the benzisothiazole **35**. A much higher efflux ratio of 10.9 than expected based on the log *D* of 2.4 was measured for the benzotriazole **36**, suggesting that this ring system is substantially more H-bond basic than benzisothiazole.

In search of further weakly H-bond basic isosteres of bicyclic aromatic groups, such as (aza)benzisoxazole, we prepared the phenyl, pyridyl, and pyrazinyl ethers **37**, **1**, and **38**. All three were devoid of P-gp mediated efflux, consistent with the very weak H-bond basicity of the oxygen atom of aromatic

https://dx.doi.org/10.1021/acs.jmedchem.9b01478
J. Med. Chem. XXXX, XXX, XXX−XXX

Table 3. Scope of the N-Substituent of Phenyl Cyclohexyl Ether Derivatives: *In Vitro* Potency, Selectivity, and log *D*

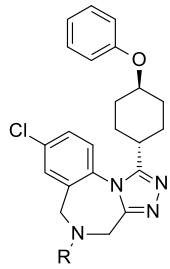

R =	H	Me			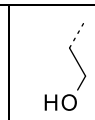	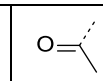	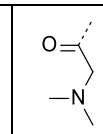	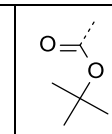		
Cpd	**42**	**37**	**43**	**44**	**45**	**46**	**47**	**48**	**49**	**50**
hV1a pK_b[a]	8.7	9.5	9.4	9.3	9.6	9.5	9.2	8.5	9.5	9.5
LE[b]	0.43	0.45	0.41	0.40	0.42	0.42	0.37	0.33	0.41	0.38
fold sel. vs hV2	523	629	535	179	1091	1055	963	19	573	445
fold sel. vs hOT	430	289	224	113	677	538	1025	17	191	190
logD	2.7	3.2	n.d.	>3.0	2.7	2.9	2.5	n.d.	3.1	4.1

[a] pK_b: negative logarithm of the equilibrium dissociation constant measured in a calcium flux functional assay. [b] LE: ligand efficiency.

ethers.[32,30] In sharp contrast, the 2-aminopyridine **39**, resulting from replacement of the ether oxygen of **1** by NH, was found to be a very good substrate of P-gp with an efflux ratio of 14. This huge difference can be attributed to the H-bond basicity of the pyridine nitrogen, which is increased by at least 1 order of magnitude,[30] as well as the additional H-bond donor; P-gp mediated efflux has been described as being particularly sensitive to the number of H-bond donors.[33] To further explore the scope of ethers, we prepared the cyclobutyl and cyclopentyl ethers **40** and **41**. By comparison with alkyl aryl ethers, dialkyl ethers are significantly better H-bond acceptors.[32,34] In line with this, **40** and **41** had slightly increased efflux ratios compared to the aryl ethers, yet well predicted by their log *D* using model 1.

After learning that even subtly increasing the polarity of the substituent R in the 4-position of the cyclohexane ring could confer P-gp mediated efflux, we chose to use the compound with the lowest efflux ratio, the phenyl cyclohexyl ether **37**, a highly potent V1a antagonist with good selectivity against hV2 and hOT receptors, as a template to explore the scope of the *N*-substituent. As summarized in Table 3 potency at the human V1a receptor was retained with a number of replacements of the *N*-methyl group, with the exception of hydrogen (**42**) and BOC (**48**). Beyond this the secondary amine **42** turned out to be a substrate of P-gp with an efflux ratio of 4.3. It should be pointed out that model 1 would predict an efflux ratio of 2.5 based on its log *D* value of 2.7, which highlights that this model based on a single parameter is certainly too simplistic to universally predict P-gp mediated efflux and that other factors such as hydrogen bonding need to be taken into account. For example in the case of **42** the increased efflux can be attributed to the introduction of the H-bond donor.[33]

Selectivity decreased with bulkier N-substituents which tended to increase lipophilicity (**43**, **44**, and **48**−**50**), whereas derivatives carrying substituents effecting a decrease in log *D* such as hydroxyethyl (**45**), acetyl (**46**), and *N*,*N*-dimethylaminoacetyl (**47**) showed enhanced selectivity, albeit at the cost of a higher molecular weight and hence decreased ligand efficiency (Table 3). Since we had shown that introduction of functionality with enhanced H-bonding capacity would increase the risk of P-gp mediated efflux, *N*-methyl substitution appeared as overall most favorable.

All but one of the *N*-methyl substituted cylcohexyl-triazolobenzodiazepine derivatives discussed above, for which P-gp data had been generated, were very potent antagonists of the human V1a receptor with K_b values below 3 nM (the full table of results is provided as Supporting Information). Among the nonsubstrates of P-gp (efflux ratio of <2) the 2-pyridyl ether **1**, which had a K_b of 0.39 nM at the human V1a receptor, clearly stood out for its outstanding functional selectivity against human V2 (3888-fold) and OT (2735-fold) receptors (Figure 4). In a diverse 120-target selectivity screen, **1** showed no significant off-target activities except for the human $5HT_{2B}$ receptor (see Supporting Information Table 3). In a functional assay **1** was found to be an antagonist of the $5HT_{2B}$ receptor with a K_b of 366 ± 97 nM (n = 3; 938-fold functional selectivity over hV1a).

https://dx.doi.org/10.1021/acs.jmedchem.9b01478
J. Med. Chem. XXXX, XXX, XXX−XXX

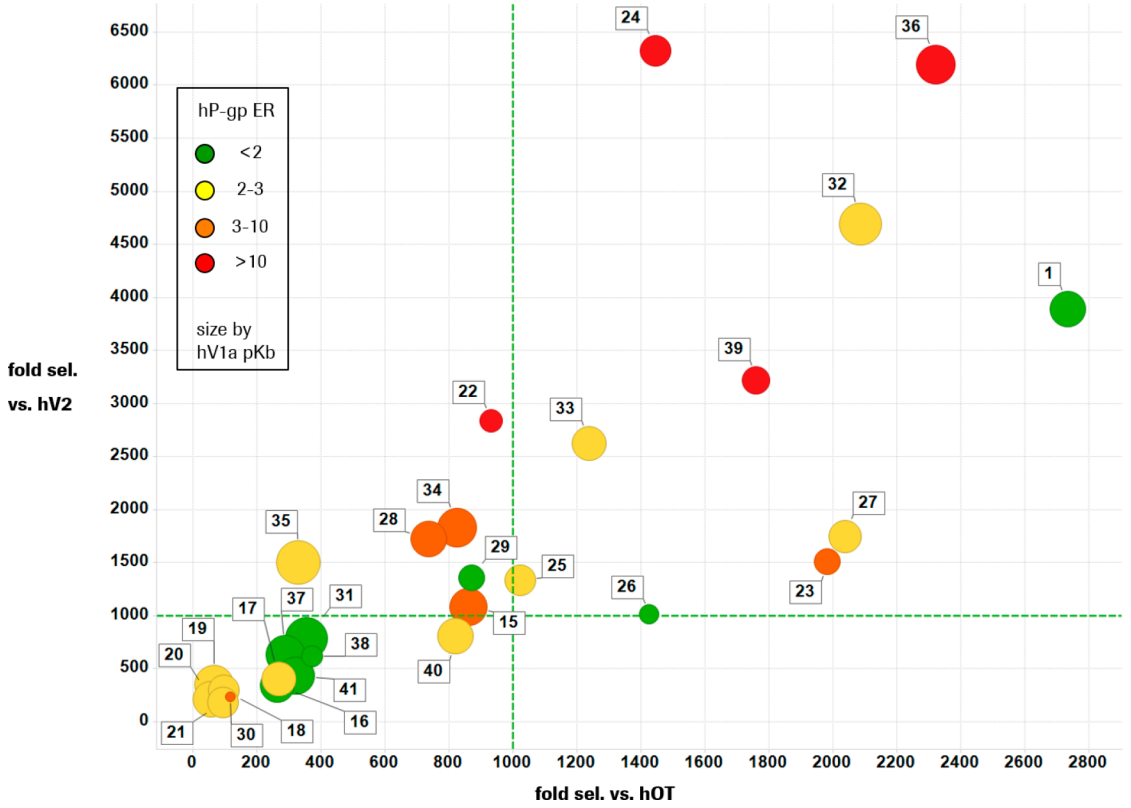

Figure 4. Selectivity of cylcohexyltriazolobenzodiazepine derivatives with P-gp data against hV2 and hOT receptors. Fold selectivity was based on functional K_b values. Green dotted lines represent 1000-fold selectivity against hOT (vertical line) and hV2 (horizontal line).

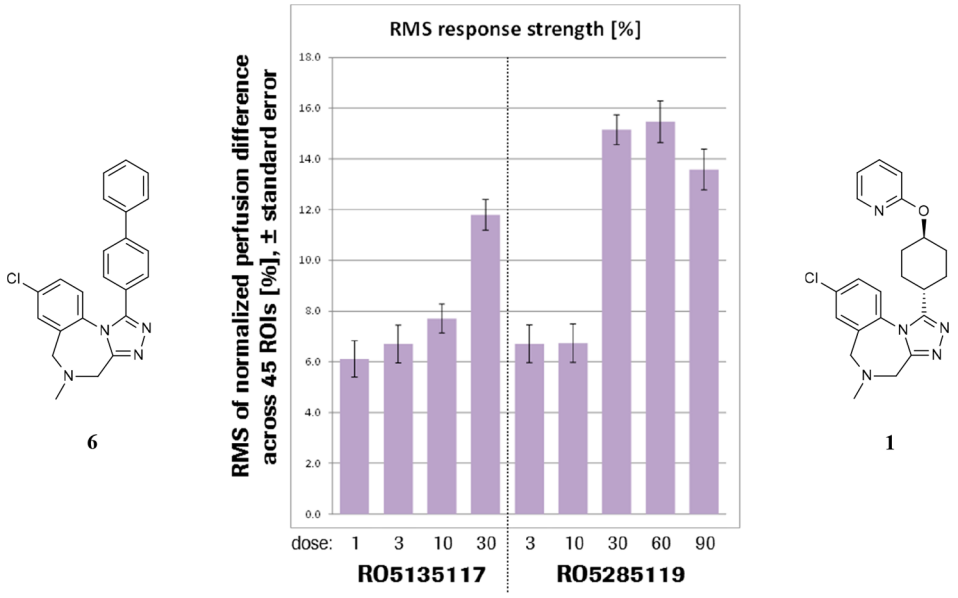

Figure 5. Dose-dependency of the overall response strength plotted as root-mean-square of normalized perfusion difference to vehicle across 45 ROIs. Values are given as group mean change ± SEM at iv doses of 1, 3, 10, and 30 mg/kg for RO5135117 (**6**) and 3, 10, 30, 60, and 90 mg/kg for RO5285119 (**1**).

In *in vivo* pharmacokinetic studies in rats, dogs, and cynomolgus monkeys **1** showed a plasma clearance which was high (close to liver blood flow) in rats but moderate or low in dogs and monkeys. Distribution volume was between 0.5 L/kg and 1.3 L/kg in the preclinical species, indicating moderate extravascular distribution, and oral bioavailability was moderate (40% in rats) to high (130% in monkeys) indicative of good oral absorption. For the prediction of human pharmacokinetics the biggest uncertainty was associated with clearance. Hepatic metabolism was believed to be the major route and was qualitatively similar across species. However, quantitative clearance scaling from *in vitro* data generated in hepatocytes was inconsistent in preclinical species, being reasonable in rat and dog but showing a large overprediction in

https://dx.doi.org/10.1021/acs.jmedchem.9b01478
J. Med. Chem. XXXX, XXX, XXX−XXX

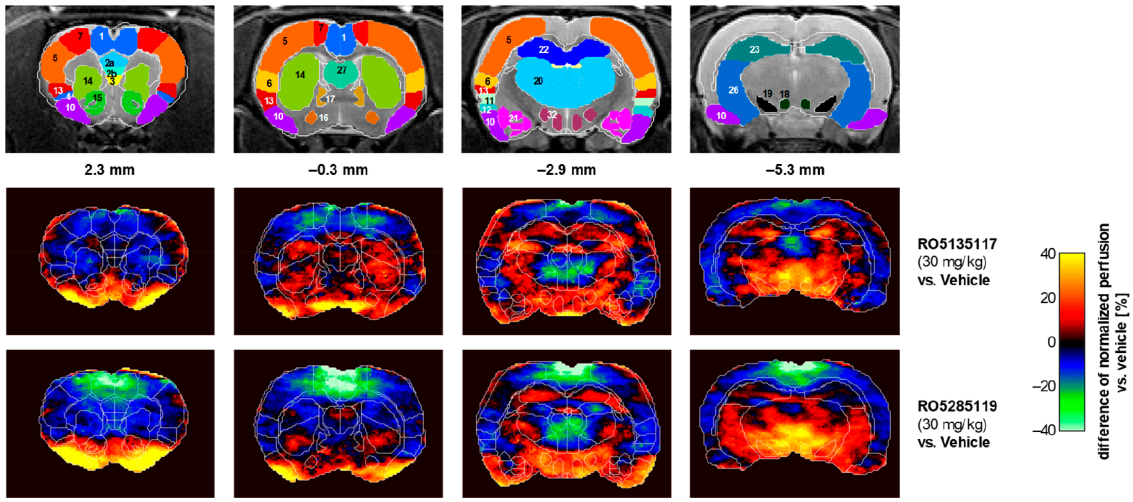

Figure 6. Activation maps showing brain (de)activation for RO5135117 (**6**) and RO5285119 (**1**) at the iv dose of 30 mg/kg. Individual columns show ROI template and group perfusion images as difference to vehicle [%] for four selected anteriorities relative to Bregma (see Experimental Section for a complete list and abbreviations of ROIs/compartments).

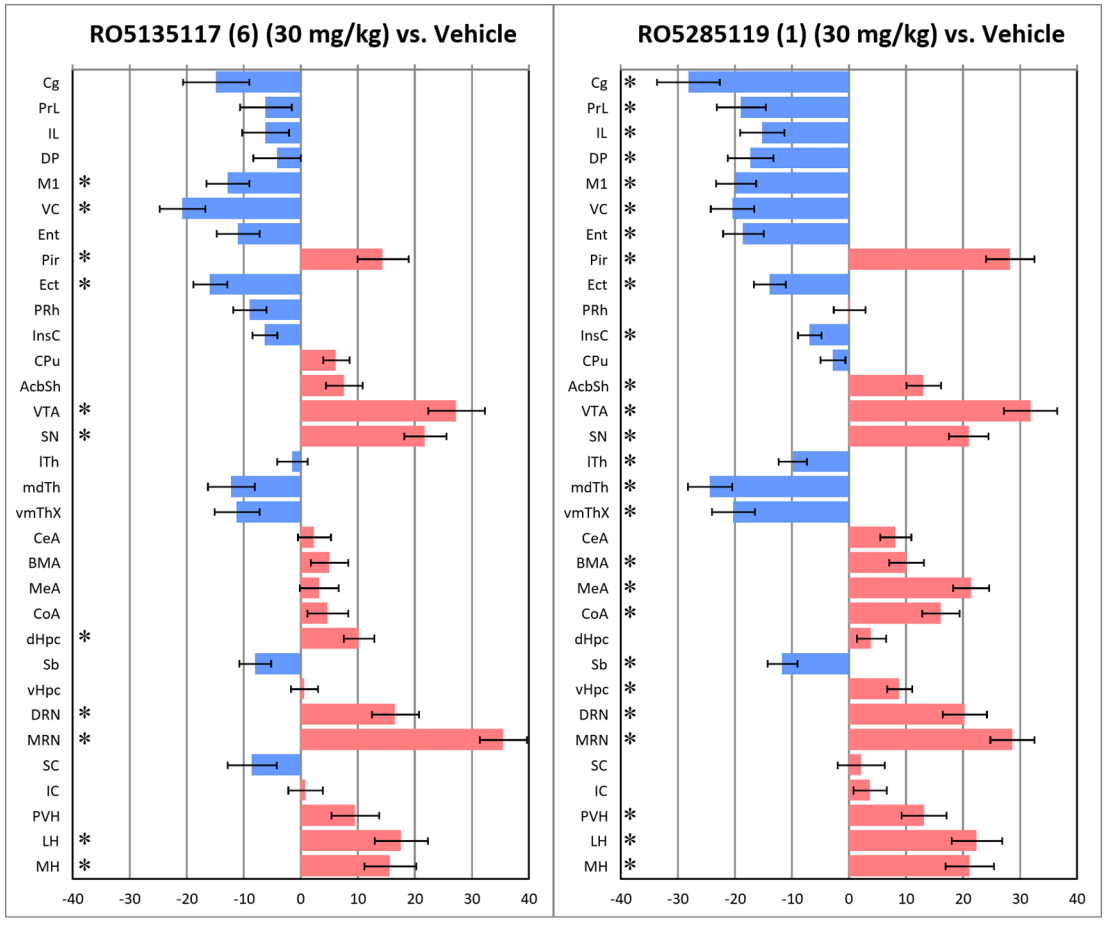

Figure 7. Perfusion profiles of RO5135117 (**6**) and RO5285119 (**1**). Values are given as difference of normalized perfusion vs vehicle [%] change ± SEM at a dose of 30 mg/kg: *$p < 0.05$; ROI-wise nested ANOVA, group [study] with FDR control at 1%. Plotted are only those ROIs with a significant response to at least one of the nine compound/dose conditions shown in Figure 5 (see Experimental Section for a complete list and abbreviations of ROIs/compartments).

monkey. Scaling from human hepatocytes predicted a clearance in the range of 4−6 mL min^{-1} kg^{-1}, but given the overprediction seen in monkey, a clearance as low as 1 mL min^{-1} kg^{-1} was considered possible. Overall, when taking the predicted human pharmacokinetics in combination with the reasonably high free fraction in plasma of 13% and the high

https://dx.doi.org/10.1021/acs.jmedchem.9b01478
J. Med. Chem. XXXX, XXX, XXX−XXX

Scheme 1. Synthesis of Triazolobenzodiazepine V1a Antagonists[a]

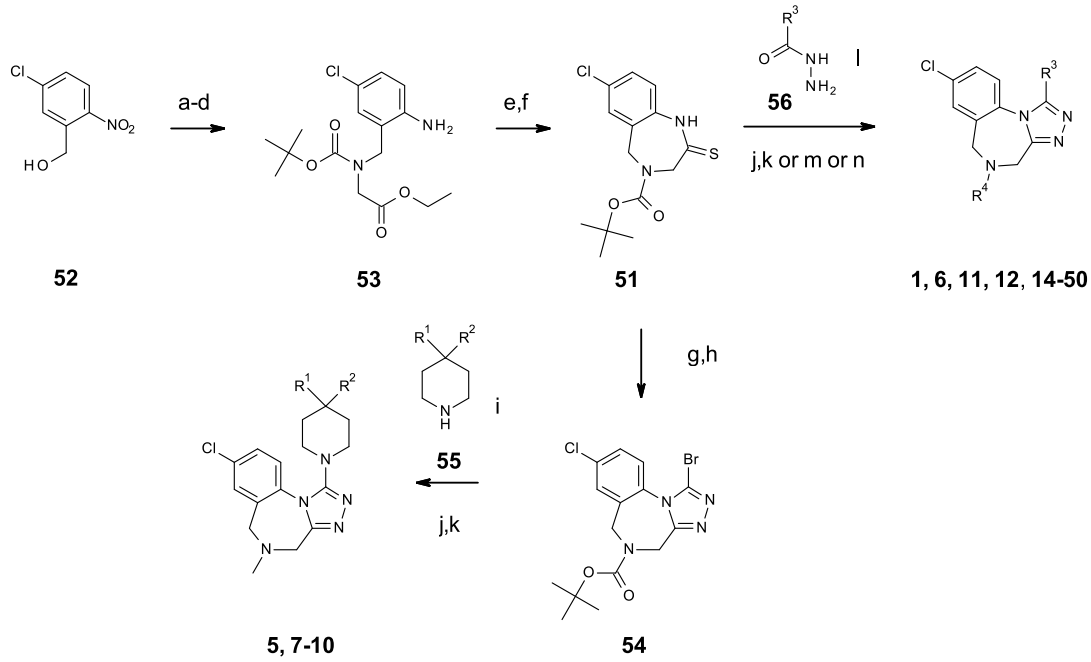

[a]Reagents and conditions: (a) $SOCl_2$, Et_3N, CH_2Cl_2, 24−32 °C, 3 h, 99%; (b) glycine ethyl ester hydrochloride, Et_3N, ethanol, reflux, 8 h, 99% crude; (c) $(BOC)_2O$, DMAP, CH_2Cl_2, 0 °C to rt, 18 h, 51%; (d) H_2 (1 bar), $ZnBr_2$, Pd/C, EtOAc, rt, 48 h, 95%; (e) KO-*t*-Bu, THF, 5 °C to rt, 3 h, 88%; (f) Lawesson's reagent, THF, reflux, 3 h, 86%; (g) $CHONHNH_2$, 1,4-dioxane, 90 °C, 18 h, 60%; (h) NBS, THF, reflux, 62%; (i) substituted piperidine **55** (10 equiv), 120 °C; (j) 1.25 M HCl in MeOH, 50 °C, 1 h; (k) aldehyde/ketone, Et_3N, MeOH, rt to reflux; $NaBH_3CN$, 0 °C to rt, or aldehyde/ketone, AcOH, MeOH, $NaBH(OAc)_3$, rt; (l) hydrazide **56**, *n*-BuOH, reflux, 16−72 h; (m) Et_3N, THF, filtration; carboxylic acid, EDC, 50 °C, 18 h; (n) R_4-Cl, Et_3N, CH_2Cl_2, rt, 18−72 h.

potency at the human V1a receptor, it was expected to be possible to achieve high levels of target engagement at a reasonable daily dose. Thus, even with a clearance of 6 mL min^{-1} kg^{-1}, which is at the higher end of the expected range, a daily dose of 10 mg was expected to achieve >70% receptor occupancy over 12 h at steady state when considering the K_b of 0.39 nM and a free fraction in plasma of 13%. Simulations are provided in the Supporting Information.

phMRI. To investigate the brain activity patterns elicited by our selective V1a antagonists, we measured region-specific alterations of perfusion as a proxy of neural activity changes using ASL-based phMRI[35] in stress-hyperresponsive rats (Fischer, F344). Acute intravenous administration of **6** and **1** resulted in consistent and dose-dependent changes of the neural activity pattern as compared to treatment with vehicle. Figure 5 shows the dose-dependency of the overall response strength measured as root-mean-square (de)activation across the regions of interest (ROIs).

At the dose of 30 mg/kg, at which the rat brain V1a receptor occupancy of **6** and **1** is estimated to be clearly greater than 90% (see Supporting Information), both compounds elicited a highly similar activity pattern comprising several cortical and subcortical brain regions. This regional change in neural activity for both compounds is depicted in Figure 6 showing brain perfusion maps in coronal orientation at selected anteriorities relative to Bregma that comprise prefrontal, entorhinal, and sensory cortices as well as regions of the basal ganglia, limbic, and brain stem nuclei.

The region-specific changes are plotted in Figure 7 as changes in normalized perfusion for 32 ROIs with significant response to at least one compound/dose condition. **1**, which showed a higher number of (de)activated areas than **6** at the selected dose, elicited a pronounced decrease in perfusion in the medial prefrontal, motor, and visual cortex on the order of −20% compared to vehicle; only in the entorhinal piriform cortex was an increase in perfusion observed. In contrast, areas of the midbrain (VTA, SN, Hyp), raphe nuclei, and amygdala showed pronounced perfusion increase upon acute dosing with **1**. Only moderate perfusion changes were observed in caudate putamen (CPU), hippocampus (dHpc), and midbrain tectum (SC, IC). Overall, the regional distribution of decreased and increased normalized perfusion was very similar for **6**, albeit at the selected dose the decrease in perfusion vs vehicle in cortical areas was generally lower. The most pronounced effect for **6** was the increase in perfusion in VTA, SN, raphe, and hypothalamic nuclei.

In phMRI the measured perfusion changes can reflect either direct local receptor engagement or regulation by interconnected upstream regions. Since V1a receptor expression is widely distributed in several subcortical and cortical brain regions, interpretation of the regional activity changes as being due to either local or circuitry engagement is not straightforward. Clearly, several areas showing V1a antagonist-induced brain activity changes possess a dense V1a receptor expression in particular in the hypothalamic and raphe nuclei, accumbens shell, hippocampus, VTA, and piriform cortex.[36] The observed perfusion changes in these brain structures hence can reflect local receptor engagement. In areas with only minor V1a receptor expression, such as the amygdala or PFC, the pronounced perfusion changes are rather induced through ascending projections from areas with high V1a receptor expression.

Taken together, we observed V1a receptor mediated effects in brain regions that are part of the social decision-making

https://dx.doi.org/10.1021/acs.jmedchem.9b01478
J. Med. Chem. XXXX, XXX, XXX−XXX

network which combines brain regions of the mesolimbic reward system with those of the social behavior network.[37] Of particular interest is the pronounced decrease in perfusion elicited by V1a antagonists in the PFC, a key node controlling social behavior. It recently has been demonstrated that increasing excitation of the PFC leads to a robust decrease in sociability in both rats and mice.[38]

CHEMISTRY

All compounds described were prepared from the common thiolactam intermediate **51** as described in Scheme 1. Chlorination of 5-chloro-2-nitrobenzyl alcohol **52** with thionyl chloride was followed by N-alkylation with glycine ethyl ester,*N*-BOC protection, and selective hydrogenation of the nitro group using zinc bromide modulated palladium on carbon[39] to give **53**. The thiolactam **51** was obtained by cylization of **53** using potassium *tert*-butoxide and treatment of the resulting lactam with Lawesson's reagent.

Condensation of **51** with formylhydrazine and bromination using *N*-bromosuccinimide gave the bromotriazole **54**. Nucleophilic aromatic substitution with an excess of a substituted piperidine **55** at elevated temperature, N-deprotection with HCl in methanol, and reductive N-methylation with paraformaldehyde and sodium cyanoborohydride gave compounds **5** and **7**−**10**.

Triazolobenzodiazepine V1a antagonists **1**, **6**, **11**, **12**, and **14**−**50** with head-groups linked to the triazole core via a carbon atom were prepared by cylocondensation of the thiolactam **51** with a hydrazide **56**. After cleavage of the BOC protecting group under acidic conditions modification of the N-substitution was effected either by reductive alkylation, amide formation using an acid and a coupling reagent such as 1-ethyl-3-(3-dimethylaminopropyl)carbodiimide (EDC), or by treatment with an acid, sulfonyl, or sulfamoyl chloride in the presence of a tertiary amine base.

CONCLUSION

To date, no centrally acting V1a receptor antagonist has received marketing authorization. Herein we describe the discovery of balovaptan **1**, a highly potent and selective brain penetrating V1a antagonist. The key to balancing potency and selectivity while minimizing P-gp mediated efflux at the blood−brain barrier was careful fine-tuning of hydrogen bond acceptor basicity. In the absence of a validated pharmacodynamic *in vivo* model for central V1a receptor antagonists, assessment of a V1a antagonist specific brain activity pattern by pharmacological magnetic resonance imaging in rats played a seminal role in strengthening confidence in the potential of the class of triazolobenzodiazepines for optimization toward a candidate drug. These effects were well in line with calculated brain V1a receptor engagement in rats based on *in vitro* potency, thus laying a solid foundation to the application of the same methodology to predict an efficacious dose in humans. Consistent with these early predictions balovaptan **1** was well tolerated and showed dose-dependent and clinically meaningful improvements in the socialization and communication domains of the Vineland-II Adaptive Behavior Scale at a dose of 4 or 10 mg/day in secondary analyses from a 12-week placebo-controlled clinical phase 2 study in adult men with moderate/severe autism spectrum disorder.[22]

Following these encouraging results, which led to a Breakthrough Therapy Designation by the U.S. FDA in January 2018,[40] balovaptan **1** entered phase 3 clinical development in adults in August 2018,[24] and a phase 2 study in children and adolescents is also currently ongoing.[23]

EXPERIMENTAL SECTION

General Information. This section contains synthesis details for key intermediates and general procedures for the preparation of the compounds discussed in the text. The specific syntheses of balovaptan **1** as well as compounds **5** and **6** are shown in this section; details for the syntheses of all other compounds discussed are in the Supporting Information. All materials for the reactions were purchased from commercial sources and used without further purification. LC−MS data were recorded on Waters UPLC/MS systems equipped with an Agilent Zorbax Eclipse Plus C18 column (2.1 mm × 30 mm, 1.8 μm, part no. 959731-902), a CTC PAL autosampler, and a Waters SQD single quadrupole mass spectrometer using electrospray ionization (ESI) modes (positive and/or negative). Chromatographic purifications were carried out using silica gel cartridges of 4−120 g (average particle size: 35−70 μm) on TELEDYNE ISCO CombiFlash Systems or by preparative RP-HPLC using a Gemini NX 3u C18 50 mm × 4.6 mm column with water/acetonitrile as eluent. LC−MS high-resolution spectra were recorded with an Agilent LC system consisting of Agilent 1290 high-pressure gradient system, a CTC PAL autosampler, and an Agilent 6520 QTOF. Ionization was performed in Agilents multimode source. The mass spectrometer was run in "2 GHz extended dynamic range" mode, resulting in a resolution of about 10 000 at m/z = 922. Mass accuracy was ensured by internal drift correction. LC−MS high-resolution data for all compounds are provided in the Supporting Information. The mean UVA/B purity of all compounds was ≥95% with three exceptions: **30**, 94.0%; **31**, 94.3%; **36**, 94.3%. ^{1}H NMR spectra were recorded on a Bruker Avance 300 MHz or an Avance III 600 MHz spectrometer, in $CDCl_3$ (δ = 7.26 ppm) or DMSO-d_6 (δ = 2.50 ppm) with all chemical shifts reported downfield from tetramethylsilane internal standard (δ in ppm). ^{1}H resonances are reported to the nearest 0.01 ppm. NMR abbreviations are as follows: s, singlet; d, doublet; t, triplet; q, quartet; quint, quintet; spt, septet; m, multiplet; br s, broad singlet. Coupling constants (J) are given in hertz (Hz).

General Procedure A: Synthesis of 4-Aryloxycyclohexane Carboxylic Acid Hydrazides. (a) Synthesis of 4-Aryloxycyclohexane Carboxylic Acid Esters. To a solution of triphenylphosphine (1.2 equiv) in dry tetrahydrofuran (0.1 M) is added diethyl azodicarboxylate (1.2 equiv) at 0 °C. After 20 min a phenol derivative (1.2 equiv) and a solution of a 4-hydroxycyclohexanecarboxylic acid ester in tetrahydrofuran (1−3 M) are added consecutively at 5 °C. After completion of addition the cooling bath is removed, and the reaction mixture is allowed to warm to room temperature and stirred for 3−18 h. The solvent is evaporated, and the residue is dissolved in ethyl acetate. The ethyl acetate solution is washed with one to two portions of 1 M aqueous sodium hydroxide solution. The aqueous layer is extracted with one to two portions of ethyl acetate. The combined organic layers are dried over anhydrous sodium sulfate and concentrated in vacuo. Purification by flash chromatography gives a 4-aryloxycyclohexane carboxylic acid ester. The main product obtained results from inversion of the absolute configuration in the 4-position.

(b) Synthesis of 4-Aryloxycyclohexane Carboxylic Acid Hydrazides. A mixture of a 4-aryloxycyclohexane carboxylic acid ester (1 equiv) and a hydrazine hydrate (5 equiv) is heated at 120 °C for 5 h. After cooling to room temperature the reaction mixture is partitioned between dichloromethane and water. The layers are separated, and the organic layer is washed with water and brine. The organic layer is dried over anhydrous sodium sulfate and concentrated in vacuo to give the crude hydrazide, which is used in the next step without further purification.

General Procedure B: Synthesis of N-Methylated Triazolobenzodiazepines. (a) Cyclocondensation. A mixture of a hydrazide derivative (1−1.5 equiv) and 7-chloro-2-thioxo-1,2,3,5-

https://dx.doi.org/10.1021/acs.jmedchem.9b01478
J. Med. Chem. XXXX, XXX, XXX−XXX

tetrahydrobenzo[*e*][1,4]diazepine-4-carboxylic acid *tert*-butyl ester **51** (1 equiv) in *n*-butanol (0.1−0.2 M) is heated at reflux for 16−72 h. After cooling to room temperature, the solvent is evaporated, and the residue is purified by flash chromatography to give a triazole derivative. In some cases partial cleavage of the *N*-BOC group is observed under these conditions.

(b) Cleavage of the *N*-BOC Group. A solution of an *N*-BOC protected triazolobenzodiazepine (1 equiv) in 1.25 M methanolic or 1.5 M ethanolic hydrogen chloride solution (10−20 equiv HCl) is heated at 50 °C for 15−60 min. After cooling to room temperature, the reaction mixture is concentrated in vacuo to give a secondary amine derivative as hydrochloride salt. The free base can be obtained by partitioning the hydrochloride salt between 1 M aqueous sodium hydroxide solution and an organic solvent such as ethyl acetate or dichloromethane. The layers are separated, and the aqueous layer is extracted with two portions of the organic solvent. The combined organic layers are dried over anhydrous sodium sulfate, filtered, and concentrated in vacuo to give the free base.

(c) Reductive N-Methylation. A mixture of an N-unsubstituted triazolobenzodiazepine as free base or as hydrochloride salt (1 equiv, 0.1−0.2 M), triethylamine (1 equiv when the hydrochloride salt is used), and paraformaldehyde (8 equiv) in methanol is heated at reflux for 2−6 h. After cooling to 0 °C sodium cyanoborohydride (2−3 equiv) is added. The reaction mixture is stirred for 3−16 h at room temperature and quenched with 1 M aqueous sodium hydroxide solution. The aqueous layer is extracted with ethyl acetate. The combined organic layers are dried over anhydrous sodium sulfate and concentrated in vacuo. Flash chromatography gives an *N*-methyl derivative.

***trans*-8-Chloro-5-methyl-1-[4-(pyridin-2-yloxy)cyclohexyl]-5,6-dihydro-4*H*-2,3,5,10*b*-tetraazabenzoazulene (1).** The title compound was obtained in 65% yield as white solid according to the general procedure B from *trans*-4-(pyridin-2-yloxy)cyclohexanecarboxylic acid hydrazide, which had been prepared according to the general procedure A from *cis*-4-hydroxycyclohexanecarboxylic acid methyl ester and 2-hydroxypyridine. ^{1}H NMR (600 MHz, $CDCl_3$): δ 8.13 (ddd, 1H, J = 5.0, 1.9, 0.6 Hz), 7.51−7.56 (m, 3H), 7.29−7.32 (m, 1H), 6.83 (ddd, 1H, J = 7.1, 5.1, 0.9 Hz), 6.66 (d, 1H, J = 8.4 Hz), 5.10 (tt, 1H, J = 10.7, 4.2 Hz), 3.11−3.99 (m, 4H), 2.83−2.95 (m, 1H), 2.48 (s, 3H), 2.23−2.39 (m, 2H), 1.85−2.21 (m, 2H), 1.78 (m, 2H), 1.41−1.58 (m, 2H). ^{13}C NMR (151 MHz, $CDCl_3$): δ 163.1, 146.9, 138.6, 132.7, 124.0, 116.5, 111.4, 72.1, 55.9, 47.7, 47.6, 43.8, 33.8, 31.4, 29.3.

8-Chloro-5-methyl-1-(1′*H*,3*H*-spiro[2-benzofuran-1,4′-piperidin]-1′-yl)-5,6-dihydro-4*H*-[1,2,4]triazolo[4,3-*a*][1,4]-benzodiazepine (5). General Procedure C. (a) *tert*-Butyl-8-chloro-1-(3*H*-spiro[isobenzofuran-1,4′-piperidin]-1′-yl)-4*H*-benzo[*f*][1,2,4]triazolo[4,3-*a*][1,4]diazepine-5(6*H*)-carboxylate. A mixture of 1-bromo-8-chloro-4*H*,6*H*-2,3,5,10*b*-tetraazabenzo[*e*]azulene-5-carboxylic acid *tert*-butyl ester **54** (0.15 g, 0.375 mmol, 1 equiv) and 3*H*-spiro[isobenzofuran-1,4′-piperidine] (0.71 g, 3.75 mmol, 1 equiv) was heated at 120 °C and stirred for 5 h. The reaction mixture was partitioned between ethyl acetate (50 mL) and saturated ammonium chloride solution. The aqueous layer was extracted with three 50 mL portions of ethyl acetate. The combined organic layers were washed with one 30 mL portion of brine, dried over Na_2SO_4, filtered, and concentrated. Trituration from ethyl acetate/*n*-heptane (1:1, 6 mL) as eluent gave the title compound (0.112 g, 59%) as a white solid. ^{1}H NMR (300 MHz, $CDCl_3$): δ 7.68−7.87 (m, 1H), 7.46−7.63 (m, 2H), 7.28−7.32 (m, 2H), 7.14−7.15 (m, 1H), 7.12−7.14 (m, 1H), 5.06 (s, 2H), 4.20−4.82 (m, 4H), 3.30−3.52 (m, 4H), 1.94−2.15 (m, 2H), 1.67−1.79 (m, 2H), 1.50 (s, 9H). MS *m*/*e*: 509 (M + H$^+$).

(b) 1′-(8-Chloro-5,6-dihydro-4*H*-benzo[*f*][1,2,4]triazolo[4,3-*a*][1,4]diazepin-1-yl)-3*H*-spiro[isobenzofuran-1,4′-piperidine] Hydrochloride. The title compound was obtained as a light brown solid (0.070 g, 86%) from *tert*-butyl 8-chloro-1-(3*H*-spiro[isobenzofuran-1,4′-piperidin]-1′-yl)-4*H*-benzo[*f*][1,2,4]triazolo[4,3-*a*][1,4]diazepine-5(6*H*)-carboxylate according to step b of the general procedure B. ^{1}H NMR (300 MHz, $CDCl_3$): δ 7.65−7.79 (m, 1H), 7.44−7.56 (m, 2H), 7.27−7.31 (m, 2H), 7.12−7.24 (m, 3H), 5.06 (s, 2H), 3.85 (s, 2H), 3.82 (s, 2H), 3.30−3.45 (m, 4H), 1.92−2.11 (m, 2H), 1.72−1.89 (m, 2H). MS *m*/*e*: 408 (M + H$^+$).

(c) 8-Chloro-5-methyl-1-(1′*H*,3*H*-spiro[2-benzofuran-1,4′-piperidin]-1′-yl)-5,6-dihydro-4*H*-[1,2,4]triazolo[4,3-*a*][1,4]-benzodiazepine (5). The title compound was obtained as a light yellow solid (0.043 g, 58%) from 1′-(8-chloro-5,6-dihydro-4*H*-benzo[*f*][1,2,4]triazolo[4,3-*a*][1,4]diazepin-1-yl)-3*H*-spiro-[isobenzofuran-1,4′-piperidine] according to step c of the general procedure B. ^{1}H NMR (600 MHz, $CDCl_3$): δ 7.73 (d, 1H, J = 8.6 Hz), 7.50 (br d, 2H, J = 8.5 Hz), 7.27−7.30 (m, 2H), 7.22 (dd, 1H, J = 5.0, 3.4 Hz), 7.18 (dd, 1H, J = 5.2, 3.5 Hz), 5.06 (s, 2H), 3.60−3.76 (m, 2H), 3.44−3.59 (m, 2H), 3.31−3.42 (m, 4H), 2.54 (br s, 3H), 2.01 (ddd, 2H, J = 13.5, 10.3, 7.1 Hz), 1.73 (br d, 2H, J = 12.5 Hz). ^{13}C NMR (151 MHz, $CDCl_3$): δ 157.0, 145.0, 139.0, 133.9, 131.5, 127.8, 127. 8, 127.4, 127.3, 123.3, 121.2, 120.7, 99.1, 84.1, 56.2, 70.9, 48.4, 45.9, 44.1, 35.5.

1-Biphenyl-4-yl-8-chloro-5-methyl-5,6-dihydro-4*H*-2,3,5,10*b*-tetraazabenzoazulene (6). The title compound was obtained as a white solid according to the general procedure B from 4-biphenylcarboxylic acid hydrazide. ^{1}H NMR (600 MHz, $CDCl_3$): δ 7.60−7.67 (m, 4H), 7.55−7.60 (m, 3H), 7.45−7.49 (m, 2H), 7.37−7.42 (m, 1H), 7.31 (dd, 1H, J = 8.5, 2.4 Hz), 6.94 (d, 1H, J = 8.6 Hz), 3.78 (br s, 2H), 3.62 (br s, 2H), 2.57 (s, 3H). ^{13}C NMR (151 MHz, $CDCl_3$): δ 152.7, 143.1, 139.9, 134.5, 133.4, 131.5, 129.3, 129.0, 129.0, 128.1, 127.5, 127.1, 125.7, 125.1, 56.3, 48.2, 44.4.

7-Chloro-2-thioxo-1,2,3,5-tetrahydrobenzo[*e*][1,4]-diazepine-4-carboxylic Acid *tert*-Butyl Ester (51). (a) 4-Chloro-2-chloromethyl-1-nitrobenzene. To a solution of 5-chloro-2-nitrobenzyl alcohol **52** (80 g, 0.42 mol, 1 equiv) and triethylamine (64 mL, 0.46 mol, 1.1 equiv) in dichloromethane (840 mL) was added dropwise thionyl chloride (34 mL, 0.46 mol, 1.1 equiv) during a period of 30 min while the internal temperature was kept below 32 °C by cooling with a water bath. The reaction mixture was stirred for 3 h. The solvent was evaporated, and the residue was triturated in warm *tert*-butyl methyl ether (970 mL). The ammonium salts were removed by filtration and the filtrate was concentrated in vacuo to give the title compound (85 g, 99%) as a brown oil which was used in the next step without purification. ^{1}H NMR (300 MHz, $CDCl_3$): δ 8.06 (d, 1H, J = 8.88 Hz), 7.73 (d, 1H, J = 2.22 Hz), 7.42−7.55 (m, 1H), 4.97 (s, 2H). MS *m*/*e*: 205 (M$^+$).

(b) (5-Chloro-2-nitrobenzylamino)acetic Acid Ethyl Ester. A mixture of 4-chloro-2-chloromethyl-1-nitrobenzene (85 g, 0.41 mol, 1 equiv), glycine ethyl ester hydrochloride (70 g, 0.50 mol, 1.2 equiv), and triethylamine (121.4 mL, 0.8665 mol, 2.1 equiv) in ethanol (1000 mL) was heated at reflux for 8 h. The solvent was evaporated, and the residue was triturated in warm *tert*-butyl methyl ether. The ammonium salts were removed by filtration, and the filtrate was concentrated in vacuo to give the title compound (111 g, 99%) as an amorphous brown solid which was used in the next step without purification. MS *m*/*e*: 273 (M + H$^+$).

(c) [*tert*-Butoxycarbonyl-(5-chloro-2-nitrobenzyl)amino]-acetic Acid Ethyl Ester. A solution of (5-chloro-2-nitrobenzylamino)acetic acid ethyl ester (110 g, 0.403 mol, 1 equiv), di-*tert*-butyl dicarbonate (180 g, 0.807 mol, 2.0 equiv), and 4-*N*,*N*-dimethylaminopyridine (2.51 g, 0.0202 mol, 0.05 equiv) in dichloromethane (1200 mL) was stirred for 2 h at 0 °C and further 16 h at room temperature. The solvent was evaporated, and the crude product was purified by flash chromatography with a cyclohexane/ethyl acetate mixture as eluent to give the title compound (76.4 g, 51%) as a light yellow viscous oil. ^{1}H NMR (600 MHz, $CDCl_3$): δ 7.95−8.06 (m, 1H), 7.58−7.63 (m, 1H), 7.37−7.43 (m, 1H), 4.87 (s, 1H), 4.81 (s, 1H), 4.18−4.24 (m, 2H), 4.04 (s, 1H), 3.93 (s, 1H), 1.48 (s, 4.7 H), 1.37 (s, 4.3 H), 1.24−1.32 (m, 3H). MS *m*/*e*: 373 (M + H$^+$).

(d) [(2-Amino-5-chlorobenzyl)-*tert*-butoxycarbonylamino]-acetic Acid Ethyl Ester (53). To a solution of [*tert*-butoxycarbonyl-(5-chloro-2-nitrobenzyl)amino]acetic acid ethyl ester (69.0 g, 0.186 mol, 1 equiv) in ethyl acetate (1200 mL) was added zinc bromide (8.5 g, 0.037 mol, 0.20 equiv). The reaction mixture was purged with argon after 15 min. After addition of the palladium catalyst (10% on

https://dx.doi.org/10.1021/acs.jmedchem.9b01478
J. Med. Chem. XXXX, XXX, XXX−XXX

activated charcoal, 7.9 g, 0.0074 mol, 0.040 equiv) the mixture was hydrogenated at ambient pressure during a period of ~48 h until ~13 L of hydrogen gas had been consumed. The catalyst was removed by filtration, and the filtrate was washed with two portions of saturated aqueous sodium bicarbonate solution and brine, each. The organic layer was dried over anhydrous sodium sulfate and concentrated in vacuo to give the title compound (60.6 g, 95.5%) as yellow waxy solid. ^{1}H NMR (600 MHz, $CDCl_3$): δ 7.05 (dd, 1H, J = 8.4, 2.2 Hz), 6.92−6.96 (m, 1H), 6.59 (br d, 1H, J = 8.4 Hz), 4.40 (s, 2H), 4.15 (q, J = 7.1 Hz, 2H), 3.78 (br s, 2H), 1.45 (br s, 9H), 1.19−1.29 (m, 3H). MS m/e: 343 ($M + H^+$).

(e) 7-Chloro-2-oxo-1,2,3,5-tetrahydrobenzo[1,4]diazepine-4-carboxylic Acid *tert*-Butyl Ester. To a solution of [(2-amino-5-chlorobenzyl)-*tert*-butoxycarbonylamino]acetic acid ethyl ester **53** (60 g, 0.18 mol, 1 equiv) in tetrahydrofuran (600 mL) was added potassium *tert*-butoxide (22 g, 0.19 mol, 1.05 equiv) in small portions at 5 °C under cooling on an ice−water batch. After addition was completed the cooling bath was removed and reaction mixture was stirred for 3 h at room temperature followed by addition of water (400 mL), saturated aqueous ammonium chloride solution (280 mL), and ethyl acetate (800 mL). After 10 min the precipitate was collected by filtration. The organic layer was separated from the filtrate, dried over anhydrous sodium sulfate, and concentrated in vacuo. The residue was combined with the precipitate, which had previously been collected by filtration, and crystallized from hot ethyl acetate to give the title compound (46 g, 88%) as a white solid. ^{1}H NMR (600 MHz, DMSO-d_6): δ 10.03−10.24 (m, 1H), 7.23−7.39 (m, 2H), 7.10 (br d, 1H, J = 8.36 Hz), 4.36−4.55 (m, 2H), 4.15−4.34 (m, 2H), 1.19−1.45 (m, 9H). MS m/e: 295 ($M - H^-$).

(f) 7-Chloro-2-thioxo-1,2,3,5-tetrahydrobenzo[*e*][1,4]-diazepine-4-carboxylic Acid *tert*-Butyl Ester (51). A mixture of 7-chloro-2-oxo-1,2,3,5-tetrahydrobenzo[1,4]diazepine-4-carboxylic acid *tert*-butyl ester (41.1 g, 0.139 mol. 1 equiv) and 2,4-bis(4-methoxyphenyl)-1,3,2,4-dithiadiphosphetane-2,4-disulfide (31.5 g, 0.0763 mol, 0.55 equiv) in tetrahydrofuran (1100 mL) was heated at reflux for 3 h. The solvent was evaporated, and the residue was triturated in *tert*-butyl methyl ether. The precipitate was removed by filtration, and the filtrate was concentrated to dryness. The residue was crystallized from hot ethanol to give the title compound (37.5 g, 86.4%) as a light yellow solid. ^{1}H NMR (600 MHz, $CDCl_3$): δ 9.34−9.87 (m, 1H), 7.28−7.45 (m, 2H), 6.97 (d, 1H, J = 8.46 Hz), 4.28−4.91 (m, 4H), 1.33−1.55 (m, 9H). MS m/e: 311 ($M - H^-$).

1-Bromo-8-chloro-4*H*,6*H*-2,3,5,10*b*-tetraazabenzo[*e*]-azulene-5-carboxylic Acid *tert*-Butyl Ester (54). (a) 8-Chloro-4*H*,6*H*-2,3,5,10*b*-tetraazabenzoazulene-5-carboxylic Acid *tert*-Butyl Ester. A mixture of 7-chloro-2-thioxo-1,2,3,5-tetrahydrobenzo-[*e*][1,4]diazepine-4-carboxylic acid *tert*-butyl ester **51** (5.7 g, 18.3 mmol, 1 equiv) and formyl hydrazine (5.5 g, 91.4 mmol, 5 equiv) in 1,4-dioxane (113 mL) was heated at 90 °C and stirred for 18 h. The solvent was evaporated. The residue was partitioned between dichloromethane (150 mL) and water (200 mL). The aqueous layer was extracted with two 75 mL portions of dichloromethane. The combined organic layers were dried over Na_2SO_4, filtered, and concentrated. Purification by column chromatography with *n*-heptane/ethyl acetate as eluent gave the title compound (3.5 g, 60%) as a white solid.

(b) 1-Bromo-8-chloro-4*H*,6*H*-2,3,5,10*b*-tetraazabenzo[*e*]-azulene-5-carboxylic Acid *tert*-Butyl Ester (54). A solution of 8-chloro-4*H*,6*H*-2,3,5,10*b*-tetraazabenzoazulene-5-carboxylic acid *tert*-butyl ester (1.3 g, 4.05 mmol, 1 equiv) and NBS (0.79 g, 4.47 mmol, 1.1 equiv) in THF (25 mL) was heated at reflux and stirred for 4 h. Purification by column chromatography with *n*-heptane/ethyl acetate as eluent gave the title compound (1.0 g, 62%) as an off-white solid.

***In Vitro* Pharmacology. Stable Cell Culture and Calcium Flux Assay Using Fluorescent Imaging.** CHO cells were stably transfected with an expression plasmid encoding one of the receptor of interest and neomycin resistance gene. The cell line expressing hV2 was additionally cotransfected with a plasmid coding for Gqs5 to redirect the cAMP signal to calcium. The cells were grown in F-12 K, containing 10% fetal bovine serum, 1% penicillin−streptomycin, 1% L-glutamate, 200 μg/mL geneticin (and 100 μg/mL hygromycin only for hV2-Gqs5) at 37 °C in a 10% CO_2 incubator at 95% humidity. Cells were plated for 24 h at 50 000 cells/well in clear-bottomed 96-well plates and were dye loaded for 60 min with 2 μM Fluo-4-AM in assay buffer. After cell washing, the plate was loaded on a fluorometric imaging plate reader (FLIPR), compound dilution series added to the cells, and the calcium signal recorded for 5 min in order to detect agonist activity. After 20 min of incubation with compound, a concentration of natural agonist (oxytocin or vasopressin depending on the receptor) giving 80% of the maximum signal was added to the plate and the calcium signal recorded for 5 min in order to detect antagonist activity of the test compound.

The calcium signal increase due to agonist activity of the compounds was fitted to the equation with variable slope Y = Bottom + (Top − Bottom)/(1 + $10^{((\log EC_{50}-X)\cdot Hillslope)}$) where Y is the % normalized fluorescence, Bottom is the minimum Y, Top is the maximum Y, EC_{50} is the concentration yielding 50% of the maximum induced fluorescence, X is the logarithm of the concentration of the test compound, and Hillslope is the Hill coefficient.

The calcium signal reduction due to the antagonist activity of the compounds was fitted to a single site competition equation with variable slope and formula Y = Bottom + (Top − Bottom)/(1 + $10^{((\log IC_{50}-X)Hillslope)}$), where Y is the % normalized fluorescence, Bottom is the minimum Y, Top is the maximum Y, IC_{50} is the concentration inhibiting 50% of the agonist-induced fluorescence, X is the logarithm of the concentration of the competing compound, and Hillslope the Hill coefficient. All compounds were tested at least 3 times in duplicate.

P-gp. Human P-glycoprotein (P-gp, MDR1) mediated efflux ratios were determined as previously described.[41]

log *D*. Water/octanol distribution coefficients or effective lipophilicities (log D) were determined as previously described.[42]

phMRI. Animals and Animal Preparation. All procedures were conducted in strict adherence to the Swiss federal regulations on animal protection and the rules of the Association for Assessment and Accreditation of Laboratory Animal Care International (AAALAC) and with the explicit approval of the local veterinary authorities. Animals were group-housed (four per cage) in a temperature- and light-controlled environment (12 h light/dark cycle) with ad libitum access to food and water. For MRI, male Fischer (F344) rats (RCC, Switzerland) weighing 300−350 g were anesthetized with isoflurane in carrier gas composed of oxygen and air (1:5) supplied to the spontaneously breathing animals initially in an inhalation box (3.5% isoflurane) and later using a face mask. During MRI isoflurane concentration was adjusted to be between 1.8% and 2.4% to maintain stable respiration rates of 50−60 breaths per minute. Rats were positioned in a Perspex cradle with the head immobilized in a stereotaxic holder, and body temperature was maintained at 37 °C via a feedback-regulated electric heating blanket. Breathing rate and concentrations of exhaled oxygen and CO_2 were monitored continuously with a capnometer (Datex, Helsinki, Finland) and recorded with a PowerLab data acquisition system (ADInstruments, Spechbach, Germany).

Magnetic Resonance Imaging. MRI was performed essentially according to previously published procedures.[35,43] In more detail, data were acquired on a 4.7 T/40 cm Bruker Biospec horizontal-bore small-animal scanner (Bruker BioSpin, Ettlingen, Germany), equipped with a 72 mm bird-cage resonator for excitation and an actively decoupled quadrature surface receiver coil (Rapid Biomedical, Rimpar, Germany) for head imaging. On scout images, the most rostral extension of the corpus callosum was used as a landmark for selecting eight coronal image planes at −10.0, −7.8, −5.3, −2.9, −1.6, −0.3, +1.0, and +2.3 mm from Bregma.[44] All subsequent images were acquired from these planes, with a field of view of 4 cm × 4 cm and a slice thickness of 1 mm. The first imaging volume was a set of RARE T_2-weighted anatomical images (TR/TE_{eff} = 1800 ms/39 ms, RARE factor 8, matrix 256 × 256).[45] Next, a T_1-weighted image series required to quantitatively calibrate perfusion readouts was obtained using an inversion−recovery snapshot FLASH sequence with 8 inversion times (TR/TE = 3400 ms/1.4 ms, matrix 128 × 64).[46]

https://dx.doi.org/10.1021/acs.jmedchem.9b01478
J. Med. Chem. XXXX, XXX, XXX−XXX

Finally, perfusion-weighted images were acquired using continuous arterial spin labeling (CASL)[47] with single-slice centered RARE readout (TR/TE 3750 ms/5.7 ms, RARE-factor 32, matrix 128 × 64, 2.5 s labeling pulse, 0.4 s postlabeling delay). Appropriate frequencies for the tagged and control images were chosen so as to minimize magnetization transfer contrast and off-resonance effects. For the assessment of compound effect three consecutive volumes of CASL perfusion images were acquired over an acquisition time of 4 min per volume followed by the compound bolus injection and a series of 9 additional volumes to track the time course of perfusion changes. Compounds **6** and **1** were formulated in saline containing Tween80 (0.3%) and 2-hydroxypropyl-β-cyclodextrin (30%), respectively, and during phMRI administered intravenously via a tail vein catheter as a bolus of 3 mL/kg volume. The following doses were tested: **6** at 1, 3, 10, and 30 mg/kg; **1** at 3, 10, 30, 60, and 90 mg/kg.

Image Processing. Images were processed and analyzed using in-house developed software written in IDL (RSI, Boulder, CO, USA) and MATLAB (The MathWorks Inc., Natick, MA, USA). The anatomical volume of each individual animal was co-registered to an in-house established rat-brain template using the open-source software SPM5 (Wellcome Trust Centre for Neuroimaging, London, U.K.). Spatial normalization comprised a 12-parameter affine and a nonlinear transform, which were then applied identically to all pharmacological images of the same subject. The template was aligned and annotated with an in-house digital atlas delineating 45 regions of interest (ROIs) adapted from the Paxinos & Watson rat-brain atlas.[44] T1 maps were calculated on a voxel-wise basis by fitting a three-parameter exponential to the image intensities across the eight inversion times.[48] These T1 maps were then combined with the related CASL images to obtain quantitative absolute perfusion maps as described elsewhere.[49,35] In order to account for possible systemic changes affecting global brain perfusion and to eliminate part of the interindividual variability, perfusion maps of each individual were normalized slicewise to the brain mean value, which was set to 100%. The temporal evolution of perfusion was quantified by fitting a three-parameter γ-variate function to the time series of each voxel, yielding the amplitude of the compound-induced perfusion changes as the parameter of interest. Amplitudes were averaged ROI-wise and pooled across hemispheres for bilateral ROIs.

ROI Labels and Abbreviations. The full list of 45 ROIs is given below. The name of each ROI is followed by its abbreviation (used for example in Figure 7) and, if applicable, the numeric label that is used in Figure 6, both in parentheses: cingulate cortex (Cg, 1); prelimbic and infralimbic cortex (PrL & IL, 2a and 2b); dorsal peduncular cortex (DP, 3); orbitofrontal cortex (OFC, 4); somatosensory cortex (SSC, 5/6); primary motor cortex (M1, 7); visual cortex (VC); entorhinal cortex (Ent); piriform cortex (Pir, 10); ectorhinal cortex (Ect, 11); perirhinal cortex (PRh, 12); insular cortex (InsC, 13); caudate putamen (CPU, 14); nucleus accumbens core and shell (AcbC & AcbSh, 15); ventral pallidum (VP, 16); bed nucleus of the stria terminalis (BNST, 17); ventral tegmental area (VTA, 18); substantia nigra (SN, 19); locus coeruleus (LC); thalamus, lateral and mediodorsal & habenula and other ventral nuclei (lTh and mdTh & Hb & vmThX, 20); amygdala, basolateral and lateral & central and basomedial & medial and cortical (BLA & LA & CeA & BMA & MeA & CoA, 21); dorsal hippocampus (dHpc, 22); posterior dorsal hippocampus (pdHpc, 23); subiculum (Sb); ventral hippocampus (vHpc, 26); septal region (Spt, 27); dorsal and ventral periaqueductal gray (dPAG and vPAG); dorsal and median raphe nuclei (DRN & MRN); superior and inferior colliculi (SC & IC); hypothalamus, lateral and median & paraventricular (LH & MH & PVH, 32).

Statistical Analyses. The data presented here are compiled from 5 studies comprising 12 active dose groups (among them 3 pairs with identical treatment in 2 studies, respectively) and 5 vehicle groups, i.e., negative control groups (1 per study), totaling 130 animals. The statistical model was an ANOVA with "dose group" as the between-subject factor of interest, which was nested within the factor "animal batch" (i.e., study) to absorb potential nuisance variability caused by general differences among batches of animals. The analysis included 10 post hoc contrasts of interest, comprising each of the 9 compound/dose combinations vs vehicle, plus an interaction contrast of the two compounds vs each other at 30 mg/kg. Readouts were least-squares estimates of group differences along with their standard errors, plus t test statistics. This analysis was conducted independently for each of the 45 ROIs, and the false discovery rate (FDR) across ROIs and contrasts (i.e., 450 single tests) was controlled at 1% using the Benjamini–Hochberg procedure.[50]

■ ASSOCIATED CONTENT

Supporting Information

The Supporting Information is available free of charge at https://pubs.acs.org/doi/10.1021/acs.jmedchem.9b01478.

Syntheses of compounds **7**–**50**; high-resolution mass spectrometry and UVA and UVB mean purity data for compounds **1** and **3**–**50**; results for RO5135117 (compound **6**) from 50-target CEREP selectivity screen; results for balovaptan (compound **1**) from 120-target CEREP selectivity screen; *in vitro* pharmacology data for compounds **1** and **3**–**50**; log D and P-gp efflux ratios for compounds **1** and **3**–**50**; prediction of free brain concentrations of compounds **1** and **6** in rodent and human; calculation of receptor occupancy; prediction of pharmacokinetics and dose in human for balovaptan (compound **1**) (PDF)

Molecular formula strings and some data (CSV)

■ AUTHOR INFORMATION

Corresponding Author

Patrick Schnider − *F. Hoffmann-La Roche Ltd., Basel, Switzerland;* orcid.org/0000-0002-5102-8818; Email: patrick.schnider@roche.com

Other Authors

Caterina Bissantz − *F. Hoffmann-La Roche Ltd., Basel, Switzerland*

Andreas Bruns − *F. Hoffmann-La Roche Ltd., Basel, Switzerland*

Cosimo Dolente − *F. Hoffmann-La Roche Ltd., Basel, Switzerland*

Erwin Goetschi − *F. Hoffmann-La Roche Ltd., Basel, Switzerland*

Roland Jakob-Roetne − *F. Hoffmann-La Roche Ltd., Basel, Switzerland*

Basil Künnecke − *F. Hoffmann-La Roche Ltd., Basel, Switzerland*

Thomas Mueggler − *F. Hoffmann-La Roche Ltd., Basel, Switzerland*

Wolfgang Muster − *F. Hoffmann-La Roche Ltd., Basel, Switzerland*

Neil Parrott − *F. Hoffmann-La Roche Ltd., Basel, Switzerland*

Emmanuel Pinard − *F. Hoffmann-La Roche Ltd., Basel, Switzerland*

Hasane Ratni − *F. Hoffmann-La Roche Ltd., Basel, Switzerland;* orcid.org/0000-0002-8151-8295

Céline Risterucci − *F. Hoffmann-La Roche Ltd., Basel, Switzerland*

Mark Rogers-Evans − *F. Hoffmann-La Roche Ltd., Basel, Switzerland*

https://dx.doi.org/10.1021/acs.jmedchem.9b01478
J. Med. Chem. XXXX, XXX, XXX−XXX

Markus von Kienlin − *F. Hoffmann-La Roche Ltd., Basel, Switzerland*
Christophe Grundschober − *F. Hoffmann-La Roche Ltd., Basel, Switzerland*

Complete contact information is available at: https://pubs.acs.org/10.1021/acs.jmedchem.9b01478

Notes

The authors declare the following competing financial interest(s): All authors are employees or former employees of F. Hoffmann-La Roche Ltd.

■ ACKNOWLEDGMENTS

We gratefully acknowledge Jens Barthold, Serge Burner, Rafael Flückiger, Sonja Keppeler, Simone Moser, Katja Ostmann, and Christian Rink for the synthesis of some of the compounds described, Andy Stucki, Muriel Schmitt, Gabrielle Py, and Alain Rudler for the *in vitro* affinity and potency assessments, Christian Bartelmus for generating high-resolution mass spectrometry data, Caroline Wyss Gramberg for recording NMR spectra, and Sebastien Debilly, Stephanie Schoeppenthau, Ciril Waelti, and Thomas Bielser for MRI measurements. Furthermore, we extend our gratitude to all teams within the Pharmaceutical Research and Early Development Department of F. Hoffmann-La Roche AG who supported this program culminating in the discovery and development of balovaptan for the treatment of autism spectrum disorder. Funding was provided by F. Hoffmann-La Roche Ltd. for this work and third-party editing assistance, which was provided by Dinakar Sambandan, Ph.D., of Envision Pharma Group, and Nick Fitch, Ph.D., CMPP, of ArticulateScience (London, U.K.).

■ ABBREVIATIONS USED

ANOVA, analysis of variance; AVP, arginine vasopressin; FDR, false discovery rate; V1a, vasopressin receptor 1a; V2, vasopressin receptor 2; OT, oxytocin; P-gp, P-glycoprotein; ROI, region of interest; HPA, hypothalamic−pituitary−adrenal; LLC-PK1 cells, porcine kidney epithelial cells; H-bond, hydrogen bond; phMRI, pharmacological magnetic resonance imaging; ASL, arterial spin-labeling

■ REFERENCES

(1) Birnbaumer, M. Vasopressin receptors. *Trends Endocrinol. Metab.* **2000**, *11*, 406−410.
(2) Koshimizu, T. A.; Nasa, Y.; Tanoue, A.; Oikawa, R.; Kawahara, Y.; Kiyono, Y.; Adachi, T.; Tanaka, T.; Kuwaki, T.; Mori, T.; Takeo, S.; Okamura, H.; Tsujimoto, G. V1a vasopressin receptors maintain normal blood pressure by regulating circulating blood volume and baroreflex sensitivity. *Proc. Natl. Acad. Sci. U. S. A.* **2006**, *103*, 7807−7812.
(3) Engelmann, M.; Landgraf, R.; Wotjak, C. T. The hypothalamic-neurohypophysial system regulates the hypothalamic-pituitary-adrenal axis under stress: an old concept revisited. *Front. Neuroendocrinol.* **2004**, *25*, 132−149.
(4) Insel, T. R. The challenge of translation in social neuroscience: a review of oxytocin, vasopressin, and affiliative behavior. *Neuron* **2010**, *65*, 768−779.
(5) Hammock, E. A.; Young, L. J. Oxytocin, vasopressin and pair bonding: implications for autism. *Philos. Trans. R. Soc., B* **2006**, *361*, 2187−2198.
(6) Kim, S. J.; Young, L. J.; Gonen, D.; Veenstra-VanderWeele, J.; Courchesne, R.; Courchesne, E.; Lord, C.; Leventhal, B. L.; Cook, E. H., Jr.; Insel, T. R. Transmission disequilibrium testing of arginine vasopressin receptor 1A (AVPR1A) polymorphisms in autism. *Mol. Psychiatry* **2002**, *7*, 503−507.
(7) Wassink, T. H.; Piven, J.; Vieland, V. J.; Pietila, J.; Goedken, R. J.; Folstein, S. E.; Sheffield, V. C. Examination of AVPR1a as an autism susceptibility gene. *Mol. Psychiatry* **2004**, *9*, 968−972.
(8) Yirmiya, N.; Rosenberg, C.; Levi, S.; Salomon, S.; Shulman, C.; Nemanov, L.; Dina, C.; Ebstein, R. P. Association between the arginine vasopressin 1a receptor (AVPR1a) gene and autism in a family-based study: mediation by socialization skills. *Mol. Psychiatry* **2006**, *11*, 488−494.
(9) Yang, S. Y.; Cho, S. C.; Yoo, H. J.; Cho, I. H.; Park, M.; Kim, B. N.; Kim, J. W.; Shin, M. S.; Park, T. W.; Son, J. W.; Chung, U. S.; Kim, H. W.; Yang, Y. H.; Kang, J. O.; Kim, S. A. Association study between single nucleotide polymorphisms in promoter region of AVPR1A and Korean autism spectrum disorders. *Neurosci. Lett.* **2010**, *479*, 197−200.
(10) Tansey, K. E.; Hill, M. J.; Cochrane, L. E.; Gill, M.; Anney, R. J.; Gallagher, L. Functionality of promoter microsatellites of arginine vasopressin receptor 1A (AVPR1A): implications for autism. *Mol. Autism* **2011**, *2*, 3.
(11) Yang, S. Y.; Kim, S. A.; Hur, G. M.; Park, M.; Park, J. E.; Yoo, H. J. Replicative genetic association study between functional polymorphisms in AVPR1A and social behavior scales of autism spectrum disorder in the Korean population. *Mol. Autism* **2017**, *8*, 44.
(12) Parker, K. J.; Oztan, O.; Libove, R. A.; Mohsin, N.; Karhson, D. S.; Sumiyoshi, R. D.; Summers, J. E.; Hinman, K. E.; Motonaga, K. S.; Phillips, J. M.; Carson, D. S.; Fung, L. K.; Garner, J. P.; Hardan, A. Y. A randomized placebo-controlled pilot trial shows that intranasal vasopressin improves social deficits in children with autism. *Sci. Transl. Med.* **2019**, *11*, No. eaau7356.
(13) Uzefovsky, F.; Shalev, I.; Israel, S.; Knafo, A.; Ebstein, R. P. Vasopressin selectively impairs emotion recognition in men. *Psychoneuroendocrinology* **2012**, *37*, 576−580.
(14) Thompson, R.; Gupta, S.; Miller, K.; Mills, S.; Orr, S. The effects of vasopressin on human facial responses related to social communication. *Psychoneuroendocrinology* **2004**, *29*, 35−48.
(15) Ratni, H.; Rogers-Evans, M.; Bissantz, C.; Grundschober, C.; Moreau, J. L.; Schuler, F.; Fischer, H.; Alvarez Sanchez, R.; Schnider, P. Discovery of highly selective brain-penetrant vasopressin 1a antagonists for the potential treatment of autism via a chemogenomic and scaffold hopping approach. *J. Med. Chem.* **2015**, *58*, 2275−2289.
(16) Umbricht, D.; Del Valle Rubido, M.; Hollander, E.; McCracken, J. T.; Shic, F.; Scahill, L.; Noeldeke, J.; Boak, L.; Khwaja, O.; Squassante, L.; Grundschober, C.; Kletzl, H.; Fontoura, P. A single dose, randomized, controlled proof-of-mechanism study of a novel vasopressin 1a receptor antagonist (RG7713) in high-functioning adults with autism spectrum disorder. *Neuropsychopharmacology* **2017**, *42*, 1914−1923.
(17) Gulliver, D.; Werry, E.; Reekie, T. A.; Katte, T. A.; Jorgensen, W.; Kassiou, M. Targeting the oxytocin system: new pharmacotherapeutic approaches. *Trends Pharmacol. Sci.* **2019**, *40*, 22−37.
(18) Johnson, P. S.; Ryckmans, T.; Bryans, J.; Beal, D. M.; Dack, K. N.; Feeder, N.; Harrison, A.; Lewis, M.; Mason, H. J.; Mills, J.; Newman, J.; Pasquinet, C.; Rawson, D. J.; Roberts, L. R.; Russell, R.; Spark, D.; Stobie, A.; Underwood, T. J.; Ward, R.; Wheeler, S. Discovery of PF-184563, a potent and selective V1a antagonist for the treatment of dysmenorrhoea. The influence of compound flexibility on microsomal stability. *Bioorg. Med. Chem. Lett.* **2011**, *21*, 5684−5687.
(19) Kakefuda, A.; Suzuki, T.; Tobe, T.; Tsukada, J.; Tahara, A.; Sakamoto, S.; Tsukamoto, S. Synthesis and pharmacological evaluation of 5-(4-biphenyl)-3-methyl-4-phenyl-1,2,4-triazole derivatives as a novel class of selective antagonists for the human vasopressin V(1A) receptor. *J. Med. Chem.* **2002**, *45*, 2589−2598.
(20) Pouzet, B.; Serradeil-Le Gal, C.; Bouby, N.; Maffrand, J. P.; Le Fur, G.; Bankir, L. Selective blockade of vasopressin V2 receptors reveals significant V2-mediated water reabsorption in Brattleboro rats with diabetes insipidus. *Nephrol., Dial., Transplant.* **2001**, *16*, 725−734.

(21) Jenkins, B. G. Pharmacologic magnetic resonance imaging (phMRI): imaging drug action in the brain. *NeuroImage* **2012**, *62*, 1072−1085.
(22) Bolognani, F.; Del Valle Rubido, M.; Squassante, L.; Wandel, C.; Derks, M.; Murtagh, L.; Sevigny, J.; Khwaja, O.; Umbricht, D.; Fontoura, P. A phase 2 clinical trial of a vasopressin V1a receptor antagonist shows improved adaptive behaviors in men with autism spectrum disorder. *Sci. Transl. Med.* **2019**, *11*, No. eaat7838.
(23) ClinicalTrials.gov. A Study to Investigate the Efficacy and Safety of RO5285119 in Participants With Autism Spectrum Disorder (ASD). https://www.clinicaltrials.gov/ct2/show/NCT02901431 (accessed Nov 26, 2019).
(24) ClinicalTrials.gov. A Study of Balovaptan in Adults With Autism Spectrum Disorder With a 2-Year Open-Label Extension. https://www.clinicaltrials.gov/ct2/show/NCT03504917 (accessed Nov 26, 2019).
(25) Detre, J. A.; Leigh, J. S.; Williams, D. S.; Koretsky, A. P. Perfusion imaging. *Magn. Reson. Med.* **1992**, *23*, 37−45.
(26) Seelig, A.; Landwojtowicz, E. Structure-activity relationship of P-glycoprotein substrates and modifiers. *Eur. J. Pharm. Sci.* **2000**, *12*, 31−40.
(27) Didziapetris, R.; Japertas, P.; Avdeef, A.; Petrauskas, A. Classification analysis of P-glycoprotein substrate specificity. *J. Drug Target.* **2003**, *11*, 391−406.
(28) Fish, P. V.; Barta, N. S.; Gray, D. L.; Ryckmans, T.; Stobie, A.; Wakenhut, F.; Whitlock, G. A. Derivatives of (3S)-N-(biphenyl-2-ylmethyl)pyrrolidin-3-amine as selective noradrenaline reuptake inhibitors: Reducing P-gp mediated efflux by modulation of H-bond acceptor capacity. *Bioorg. Med. Chem. Lett.* **2008**, *18*, 4355−4359.
(29) El Tayar, N.; Testa, B.; Carrupt, P. A. Polar intermolecular interactions encoded in partition coefficients: an indirect estimation of hydrogen-bond parameters of polyfunctional solutes. *J. Phys. Chem.* **1992**, *96*, 1455−1459.
(30) Berthelot, M.; Laurence, C.; Safar, M.; Besseau, F. Hydrogen-bond basicity pKHB scale of six-membered aromatic N-heterocycles. *J. Chem. Soc., Perkin Trans. 2* **1998**, 283−290.
(31) Kenny, P. W.; Montanari, C. A.; Prokopczyk, I. M.; Ribeiro, J. F.; Sartori, G. R. Hydrogen bond basicity prediction for medicinal chemistry design. *J. Med. Chem.* **2016**, *59*, 4278−4288.
(32) Abraham, M. H.; Duce, P. P.; Prior, D. V.; Barratt, D. G.; Morris, J. J.; Taylor, P. J. Hydrogen bonding. Part 9. Solute proton donor and proton acceptor scales for use in drug design. *J. Chem. Soc., Perkin Trans. 2* **1989**, 1355−1375.
(33) Hitchcock, S. A. Structural modifications that alter the P-glycoprotein efflux properties of compounds. *J. Med. Chem.* **2012**, *55*, 4877−4895.
(34) Berthelot, M.; Besseau, F.; Laurence, C. The hydrogen-bond basicity pKHB scale of peroxides and ethers. *Eur. J. Org. Chem.* **1998**, *1998*, 925−931.
(35) Bruns, A.; Kunnecke, B.; Risterucci, C.; Moreau, J. L.; von Kienlin, M. Validation of cerebral blood perfusion imaging as a modality for quantitative pharmacological MRI in rats. *Magn. Reson. Med.* **2009**, *61*, 1451−1458.
(36) Smith, C. J.; Poehlmann, M. L.; Li, S.; Ratnaseelan, A. M.; Bredewold, R.; Veenema, A. H. Age and sex differences in oxytocin and vasopressin V1a receptor binding densities in the rat brain: focus on the social decision-making network. *Brain Struct. Funct.* **2017**, *222*, 981−1006.
(37) O'Connell, L. A.; Hofmann, H. A. The vertebrate mesolimbic reward system and social behavior network: a comparative synthesis. *J. Comp. Neurol.* **2011**, *519*, 3599−3639.
(38) Benekareddy, M.; Stachniak, T. J.; Bruns, A.; Knoflach, F.; von Kienlin, M.; Kunnecke, B.; Ghosh, A. Identification of a cortico-habenular circuit regulating socially directed behavior. *Biol. Psychiatry* **2018**, *83*, 607−617.
(39) Wu, G.; Huang, M.; Richards, M.; Poirier, M.; Wen, X.; Draper, R. W. Novel ZnX_2-modulated Pd/C and Pt/C catalysts for chemoselective hydrogenation and hydrogenolysis of halogen-substituted nitroarenes, alkenes, benzyl ethers, and aromatic ketones. *Synthesis* **2003**, *2003*, 1657−1660.
(40) FDA. Roche's Autism Drug Balovaptan Granted Breakthrough Therapy Designation. https://www.fdanews.com/articles/185437-roches-autism-drug-balovaptan-granted-breakthrough-therapy-designation (accessed Nov 26, 2019).
(41) Poirier, A.; Weetall, M.; Heinig, K.; Bucheli, F.; Schoenlein, K.; Alsenz, J.; Bassett, S.; Ullah, M.; Senn, C.; Ratni, H.; Naryshkin, N.; Paushkin, S.; Mueller, L. Risdiplam distributes and increases SMN protein in both the central nervous system and peripheral organs. *Pharmacol. Res. Perspect.* **2018**, *6*, No. e00447.
(42) Schnider, P.; Dolente, C.; Stalder, H.; Martin, R. E.; Reinmüller, V.; Marty, R.; Wyss Gramberg, C.; Wagner, B.; Fischer, H.; Alker, A. M.; Müller, K. Modulation of pharmacologically relevant properties of piperidine derivatives by functional groups in an equatorial or axial β-position to the amino group. *ChemBioChem* [Online early access]. DOI: 10.1002/cbic.201900474. Published Online: Sep 6, **2019**. https://onlinelibrary.wiley.com/doi/abs/10.1002/cbic.201900474 (accessed Nov 26, 2019).
(43) Bruns, A.; Mueggler, T.; Kunnecke, B.; Risterucci, C.; Prinssen, E. P.; Wettstein, J. G.; von Kienlin, M. "Domain gauges": A reference system for multivariate profiling of brain fMRI activation patterns induced by psychoactive drugs in rats. *NeuroImage* **2015**, *112*, 70−85.
(44) Paxinos, G., Watson, C., Eds. *The Rat Brain in Stereotaxic Coordinates*; Academic Press: San Diego, CA, 1998.
(45) Hennig, J.; Nauerth, A.; Friedburg, H. RARE imaging: a fast imaging method for clinical MR. *Magn. Reson. Med.* **1986**, *3*, 823−833.
(46) Haase, A.; Frahm, J.; Matthaei, D.; Hanicke, W.; Merboldt, K. D. FLASHimaging - rapid NMRimaging using low flip-angle pulses. *J. Magn. Reson.* **1986**, *67*, 258−266.
(47) Williams, D. S.; Detre, J. A.; Leigh, J. S.; Koretsky, A. P. Magnetic resonance imaging of perfusion using spin inversion of arterial water. *Proc. Natl. Acad. Sci. U. S. A.* **1992**, *89*, 212−216.
(48) Deichmann, R.; Hahn, D.; Haase, A. Fast T1 mapping on a whole-body scanner. *Magn. Reson. Med.* **1999**, *42*, 206−209.
(49) Alsop, D. C.; Detre, J. A. Reduced transit-time sensitivity in noninvasive magnetic resonance imaging of human cerebral blood flow. *J. Cereb. Blood Flow Metab.* **1996**, *16*, 1236−1249.
(50) Benjamini, Y.; Hochberg, Y. Controlling the false discovery rate: a practical and powerful approach to multiple testing. *J. R. Statist. Soc. B* **1995**, *57*, 289−300.

https://dx.doi.org/10.1021/acs.jmedchem.9b01478
J. Med. Chem. XXXX, XXX, XXX−XXX